Muhammed Furkan ERMAN

Theoretical Investigation and Modeling of Various Shaped Planar Coils for Induction System Applications

AGU 2019

Theoretical Investigation and Modeling of Various Shaped Planar Coils for Induction System Applications

A THESIS
SUBMITTED TO THE DEPARTMENT OF ELECTRICAL AND COMPUTER ENGINEERING
AND THE GRADUATE SCHOOL OF ENGINEERING AND SCIENCE
OF ABDULLAH GUL UNIVERSITY
IN PARTIAL FULFILLMENT OF THE REQUIREMENTS
FOR THE DEGREE OF
MASTER

By
Muhammed Furkan ERMAN
December 2019

Theoretical Investigation and Modeling of Various Shaped Planar Coils for Induction System Applications

A THESIS
SUBMITTED TO THE DEPARTMENT OF ELECTRICAL AND COMPUTER ENGINEERING
AND THE GRADUATE SCHOOL OF ENGINEERING AND SCIENCE OF ABDULLAH GUL UNIVERSITY
IN PARTIAL FULFILLMENT OF THE REQUIREMENTS
FOR THE DEGREE OF
MASTER

By
Muhammed Furkan ERMAN
December 2019

SCIENTIFIC ETHICS COMPLIANCE

I hereby declare that all information in this document has been obtained in accordance with academic rules and ethical conduct. I also declare that, as required by these rules and conduct, I have fully cited and referenced all materials and results that are not original to this work.

Muhammed Furkan ERMAN

REGULATORY COMPLIANCE

M.Sc. thesis titled **“Theoretical Investigation and Modeling of Various Shaped Planar Coils for Induction System Applications"** has been prepared in accordance with the Thesis Writing Guidelines of the Abdullah Gül University, Graduate School of Engineering & Science.

Prepared By	Advisor
Muhammed Furkan ERMAN	Asst. Prof. Dr. Veli Tayfun KILIÇ

Head of the Electrical and Computer Engineering Program

Prof. Dr. Vehbi Çağrı GÜNGÖR

ACCEPTANCE AND APPROVAL

M.Sc. thesis titled “Theoretical Investigation and Modeling of Various Shaped Planar Coils for Induction System Applications" and prepared by Muhammed Furkan Erman has been accepted by the jury in the Electrical and Computer EngineeringGraduate Program at Abdullah Gül University, Graduate School of Engineering & Science.

16/12/2019
(Thesis Defense Exam Date)

JURY:

Advisor: Asst. Prof. Dr. Veli Tayfun KILIÇ

Member: Assoc. Prof. Dr. Günyaz ABLAY

Member: Assoc. Prof. Dr. Mustafa TÜRKMEN

APPROVAL:

The acceptance of this M.Sc. thesis has been approved by the decision of the Abdullah Gül University, Graduate School of Engineering & Science, Executive Board dated ….. /….. / …….. and numbered ……..……. .

…….. /…….. / ……..
(Date)
Graduate School Dean
Name-Surname, Signature

ABSTRACT

Theoretical Investigation and Modeling of Various Shaped Planar Coils for Induction System Applications

Muhammed Furkan ERMAN
MSc. in Electrical and Computer Engineering Department
Supervisor: Asst. Prof. Dr. Veli Tayfun KILIÇ
December 2019

Heating occupies an important place in industry. With the development of technology, in today's world there are different kinds of heating methods that are being widely used including resistive and infrared heating, etc. Among these methods, induction heating is increasingly becoming more popular. One of the most important parts of induction heating systems is coil. Coil creates magnetic field when electrical power is applied on and current flows through it. It is possible to see different coil shapes in industry such as circular and square shapes, etc. Analytical investigation of these coil shapes is possible by using existing formulas in the literature. However, due to the production difficulties of sharp corners or on purpose, it is inevitable to face rounded corners in coil geometries having sharp corners such as square shaped coils, which is called squircle coil when its corners are rounded. Since coil shape is different than its original form, magnetic flux density created at the center of the coil is not the same. In this study, a gap in literature is filled with derivation of required formulas to examine such coils analytically. Obtained derivations were verified by calculating magnetic flux densities created by squircle and triangular shaped coils. For each coil shape simulations were repeated for two different cases. Similarly, for each case simulations were renewed for three different coil sizes, and for each size 5 different amounts of rounding were selected. In the first case, arcs are assumed to be parts of a circle whose center is coinciding with the center of the coil. In case 1, magnetic flux densities created by coils are calculated by using both proposed and traditional formulas. In the second case, on the other hand, arcs are set to be parts of circles positioned at different locations such that their centers do not coincide with the coil center. In case 2, total length of the coil for

different amounts of rounding was kept constant to see the effect of the rounding on created magnetic field density. Also, calculations in this case are obtained by using only the proposed method. After calculations of magnetic flux densities, results were supported with three-dimensional electromagnetic simulations. Comparison of the results found with analytical calculations and simulations show that the maximum error between the proposed method and traditional method; and the maximum error between the proposed method and simulations are both less than 1%.

Keywords: Induction Heating, Squircle Coil, Triangular Coil, Magnetic Flux Density, Rounded Corners.

ÖZET

İndüksiyon Sistemi Uygulamaları için Farklı Düzlemsel Bobin Şekillerinin Teorik Olarak İncelenmesi ve Modellenmesi

Muhammed Furkan ERMAN
Elektrik ve Bilgisayar Mühendisliği Bölümü Yüksek Lisans
Tez Yöneticisi: Dr. Veli Tayfun KILIÇ
Aralık 2019

Isıtma endüstride önemli bir yer kaplar. Teknolojinin gelişmesiyle birlikte, günümüz dünyasında, resistif ve kızılötesi ile ısıtma yöntemleri de dahil olmak üzere yaygın olarak kullanılan birçok ısıtma yöntemi vardır. Bu yöntemler arasında, indüktif ısıtma giderek daha popüler hale gelmektedir. İndüktif ısıtma sistemlerinin en önemli parçalarından biri bobindir. Bobin, elektrik enerjisi uygulandığında ve üzerinden akım geçtiğinde manyetik alan oluşturur. Endüstride dairesel, kare vb. şekillerde farklı bobin şekillerini görmek mümkündür. Literatürde mevcut formüller kullanılarak bu bobin şekillerinin analitik incelenmesi yapılabilmektedir. Ancak üretim zorluklarından veya sağladığı avantajlardan dolayı kare bobin gibi köşeleri keskin olan bobinlerin köşelerinin yuvarlanması kaçınılmazdır. Köşeleri yuvarlanmış bobin yapısı orijinal yapısından farklı olduğundan dolayı oluşturduğu manyetik akı yoğunluğu aynı olmamaktadır. Bu tezde, bu tür bobinlerin analitik olarak incelenebilmesi için gerekli formüllerin türetilmesi ile literatürdeki boşluk doldurulmuştur. Bulunan formüller köşeleri yuvarlanmış kare ve üçgen şeklindeki bobinlerin oluşturduğu manyetik akı yoğunluğu hesaplanarak doğrulanmıştır. Her iki bobin şekli modellenerek simule edilmiştir. Her bir şekil için 3 farklı boyut ve her boyut için 5 farklı yuvarlama miktarı seçilmiştir. İlk durumda, yuvarlanan köşe merkezlerinin bobinin merkezi ile çakıştığı varsayılmıştır. Bu sayede bobin merkezinde oluşan manyetik akı yoğunluğu hem geleneksel formüller ile hem de bu tezde türetilen formüller ile hesaplanmıştır. İkinci durumda ise yaylar, merkezleri bobin merkeziyle çakışmayacak şekilde farklı konumlara yerleştirilmiş çemberin parçaları olarak ayarlanmıştır. İkinci durumda, yuvarlamanın yaratılan manyetik alan yoğunluğu üzerindeki etkisini görmek için farklı miktarlarda yuvarlama için bobinin

toplam uzunluğu sabit tutulmuştur. Bu durumda hesaplamalar sadece bu çalışmada türetilen formüller ile yapılabilmektedir. Manyetik akı yoğunluklarının hesaplanmasından sonra, sonuçlar üç boyutlu elektromanyetik simülasyonlarla desteklenmiştir. Bulunan sonuçların analitik hesaplamalar ve simülasyonlarla karşılaştırılması, önerilen yöntem ile geleneksel yöntem arasındaki ve önerilen yöntem ile simülasyonlar arasındaki maksimum hatanın % 1'den az olduğunu göstermiştir.

Anahtar kelimeler: İndüksiyon Isıtma, Karesel Bobin, Üçgen Bobin, Manyetik Akı Yoğunluğu, Yovarlanmış Köşeler.

Acknowledgements

I would like to express my sincere appreciation to my advisor Asst. Prof. Dr. Veli Tayfun KILIÇ for his excellent support, assistance and mostly for the great patience he endured to assist me throughout my master degree. Patience is the highest degree a teacher offers to his student.

I would like to thank my friends and my family members particularly my wife Seda Küçükşahin ERMAN for her encouragement.

Table of Contents

List of Figures

List of Tables

Chapter 1

Introduction

Heating occupies an important place in human life and in industry. It has been used since discovery of fire in ancient history. For example, iron is heated up and then cooled for being hardened in production of swords. This was one of the mostly used techniques since the Iron Age. However, it is a milestone for the humanity to carry fire. With invention of modular device products humans can carry and bring fire to everywhere, which widens to use fire. Despite advantages of being modular, heating efficiency of primitive methods is very low. Efficiency of heating systems has been increased as a result of discovery of new types of fuels and energy sources. After invention of electricity, in the last few decades with developments in power and control systems efficiency of heating systems (both for industrial and consumer electronics) has been increased further. Efficiency of heating systems operating with different energy sources and fuel types is given in Table 1.1.

Technology	**Efficiency**
Induction	76%
Conventional Electric	42%
Natural Gas	30%

Table 1.1 Efficiency of different heating systems. [1]

Today, because it is one of the cheapest and cleanest energy types, electrical energy is the most widely used energy in heating systems. In addition, heating systems that use electrical energy are highly efficient and safe. On the other hand, although they are both use electrical energy, two types of electrical heating systems exist that are resistive and induction heating systems.

1.1 Resistive Heating

In resistive heating systems, heat energy arisen from self-heating of a system part (resistor) is transferred to other system parts and materials to be heated. In those systems, self-heating of resistor and transfer of heat energy with contact are essential. In resistive heating systems, nickel-chrome wire is one of the most widely used materials for the resistor. Nickel-chrome is an alloy composed of nickel and chrome elements. [2-5] In resistive heating systems, wires are made of nickel-chrome alloy with various nickel and chrome percentages because nickel-chrome resistors are immune to corrosion and oxidations. In addition, nickel-chrome is a highly resistive material such that it can quickly heat up even when electrical currents with very small intensities flow over it. Despite its high self-resistance, another property of nickel-chrome alloy is being persistent to high temperatures. The wires made of nickel-chrome alloy are also called Nichrome wires.

Self-resistance of a resistor in resistive heating systems and in electric circuits depends on its geometry and material. Self-resistance of a wire is calculated by (1.1.1), where ℓ is the length, A is the cross-sectional area that is perpendicular to flow of current, and ρ is the resistivity of the material. As seen, resistance of a wire is directly proportional to its length and resistivity but resistance is inversely proportional to cross-sectional area [6].

$$R = \frac{\rho \ell}{A} \tag{1.1.1}$$

Resistors are usually preferred to be used for home-type and industrial hobs, ovens, heaters, etc. They are designed and manufactured to obtain best heating performance together with being safe and cheap. For the highest heating efficiency different resistor structures were developed [7,8]. Depending on application, restrictions and necessities change and these restrictions and necessities determine structure of a resistor. An exemplary heating element (resistor) exists in a resistive heating system is shown in Figure 1.1.1. As seen in the figure, resistor is formed by winding a wire in a two-dimensional (2D) spiral shape. By this way, length of the wire is increased while its cross-sectional area remains low. Therefore, resistance of the wire becomes high in a limited region. Since amount of heat energy appeared on the system is proportional to power loss in the resistor and thus resistance of the resistor [9], such spiral wire windings

that enable high resistance are commonly used in heaters where heating is achieved from a surface.

Figure 1.1.1 Exemplary heating element having a winding wire in a two-dimensional spiral shape used in resistive heating systems [10].

1.2 Induction Heating

Induction heating, another electrical heating method, is provided by the hysteresis and eddy currents generated by the magnetic field formed by the high frequency alternating current on the magnetic materials [11]. When alternating current is applied to a coil, a variable magnetic field is generated around the coil and the generated time-varying magnetic field induces a voltage on other materials in the magnetic field. These phenomena are described by Ampere's circuital law and Faraday's law, respectively, that are two of the Maxwell's equations [12]. The induced voltage on the material exposed to the magnetic field causes the induction currents (eddy currents) to flow in the materials according to Lenz's law [13]. Maxwell equations and Lenz's law are given in (1.2.1) and (1.2.2), respectively.

$$\nabla x\vec{E} = -\frac{\partial \vec{B}}{\partial t} \quad \textbf{(1.2.1a)}$$

$$\nabla x\vec{H} = \vec{J} + \frac{\partial \vec{D}}{\partial t} \quad \textbf{(1.2.1b)}$$

$$\nabla x\vec{B} = 0 \quad \textbf{(1.2.1c)}$$

$$\nabla x\vec{D} = \rho \quad \textbf{(1.2.1d)}$$

$$\varepsilon = -\frac{d\Phi_B}{dt} \quad \textbf{(1.2.2)}$$

Here, $\vec{E}$ and $\vec{H}$ are electrical and magnetic fields, respectively. Also, $\vec{B}$ is the magnetic flux density and $\vec{D}$ is the electrical displacement vector. Similarly, $\vec{J}$ and p stand for current and charge densities, respectively. As seen in (1.2.1b), magnetic fields can be produced either by a time-varying electrical displacement vector, which is related with electrical field, or by a current. The generated magnetic fields are looping magnetic fields, i.e., they are closing upon themselves. On the other hand, as can be deduced from (1.2.1a), an electrical field can be produced by varying magnetic flux density, which is related with magnetic field, and this produced looping electrical fields.

The Lenz's law is an integral form of Maxwell's equations. Its derivation is given below.

$$\oint \vec{E}.d\vec{s} = -\frac{d\Phi_B}{dt} \qquad \textbf{(1.2.3)}$$

Lenz's Law states that the direction of produced emf is in the direction of the current that generates the magnetic flux to resist the change of the magnetic flux passing through the area surrounded by the current loop. This means that the direction of the back EMF of an induced field opposes the changing current that is its cause.

The induced currents may reach to high values in suitable environments depending on system geometry, material types, and so on. For instance, in induction hobs since planar coils are located on the surface, vessels to be heated are placed on top of the coils perpendicular to the magnetic flux generated by the coil with a very short distance between. By this way, magnetic flux produced by the coils is captured as much as possible thus the induced current on the vessel is increased. However, for the vessel in induction hobs stainless steel is one of the mostly preferred materials because stainless steel has a very high permeability and its resistivity is higher than the other metals used for vessel production such as copper, aluminum, etc.

High eddy currents and high resistance the heating materials are important for efficient heating in an induction hob. Although in other applications, such as in an electrical wire heating power causes loss, in induction heating systems it is desired to have high power turning into heat on the object. A simple induction heating system, in which planar coils are located on the surface, is illustrated in Figure 1.2.1. As seen in the figure, magnetic fields produced from the coils couple to the vessel. Eddy currents are induced on the vessel as a result of coupling and because of finite conductivity of the vessel material it heats up. In short, in induction heating systems electrical energy is

transferred wirelessly from a coil to a vessel. Because of finite conductivity of the vessel and with help of the induced eddy currents transferred electrical energy is turned out to be heat energy on the vessel. Induction heating systems can reach to very high efficiencies thanks to wireless power transmission. Besides finite conductivity of the metals, in induction heating systems hysteresis losses on magnetic metal materials also cause some heating [14].

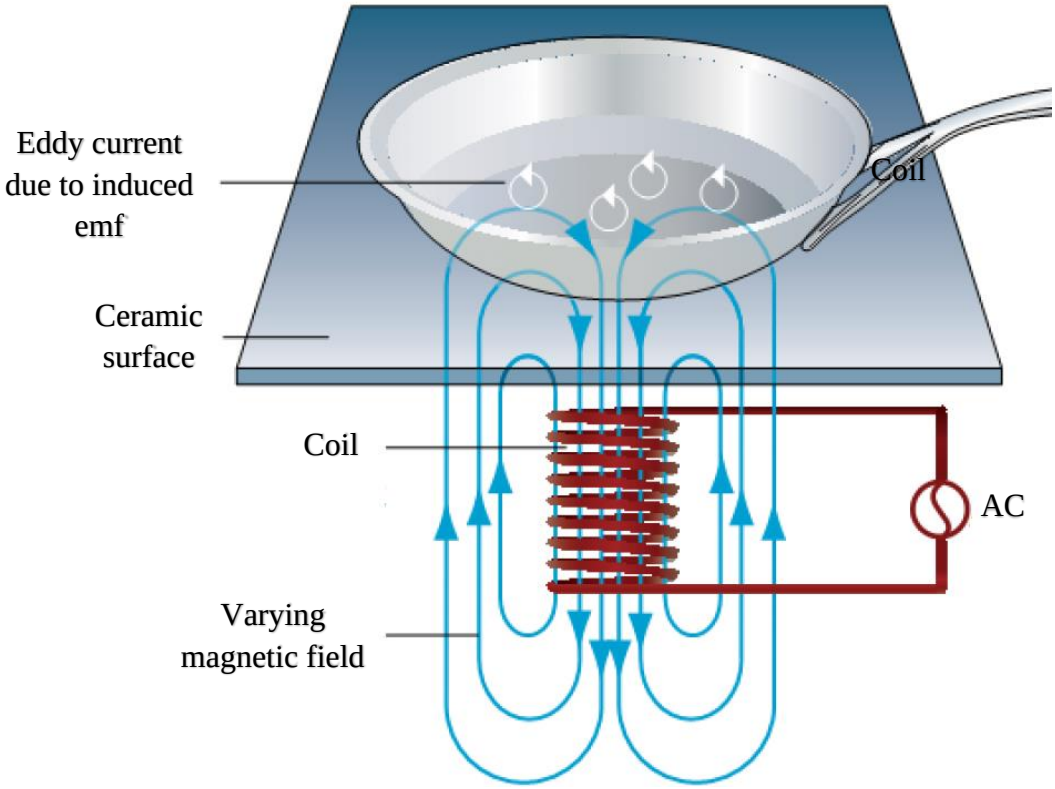

Figure 1.2.1 Creation of eddy currents when alternating current is applied to a coil in an induction hob [15].

Due to the advantages of fast heating, power control by changing frequency, high efficiency, constant, precise, and safe heating, and being pollution free [16], induction heating systems have been used in several industrial and household applications including cooking, metal melting, and hardening, etc. [11]. Working principle of induction heating systems is based on flowing alternating current through a coil and creating magnetic field [17]. Since, heat energy arise on the heating material is proportional to eddy current induced on it, high currents are required to flow on the coil. Therefore, induction heating systems should be capable of handling high currents and fast switching of power elements. For that, induction heating systems usually consist of different parts. For example, an induction hob is composed of three parts. They are power electronics circuit, control circuit, and coil. System parts of an induction hob are illustrated in Figure 1.2.1.1.

Power circuit is for supplying required electrical current to the coil. It rectifies the city line signal and adjusts the signal frequency to a desired level. On the other hand, control circuitry regulates these operations. It controls power circuitry especially in case of changes in load with time. As the third part, coils are responsible for producing magnetic flux. An alternating current supplied by the power circuitry flows on the coil. As a result, magnetic flux is generated and couples to a vessel. In other words, coils transform electrical energy into electromagnetic energy, which is crucial for wireless energy transfer in induction systems. Parts of an induction heating system are described below in more details.

1.2.1 Power Electronic and Control Circuits

In an induction heating system power electronic and control circuits operate synchronously. Electrical circuit of an exemplary induction hob is shown in Figure 1.2.1.1. As seen, power electronic circuit is composed of rectifier, EMC filter, and inverter [18].

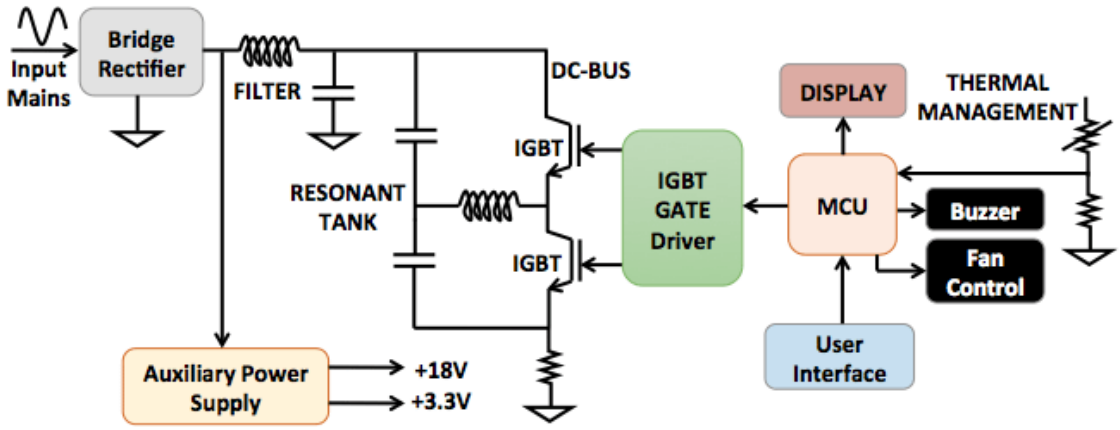

Figure 1.2.1.1 Exemplary induction hob electrical structure [19].

Rectifier is an electrical circuit consisting of one or more semiconductor elements (e.g. diodes) used to convert alternating current to direct current. The purpose of this conversion is to supply invertor circuitry by using single phase or three phase grid line [18]. Electromagnetic compatibility (EMC) filter is another part of the power supply circuitry. EMC can be defined as any effect provided in the creation, transmission and reception of electromagnetic energy, which does not constitute an electromagnetic interference [20]. It is inevitable that sources operating with alternating currents generate

electromagnetic waves. In application, sources generating electromagnetic waves are called attackers and devices exposed to and affected by the produced waves are named victims [21]. The source may also be affected and become a victim. However, this interaction prevents systems from operating as desired. To overcome the problem there are three main methods that are preventing or suppressing the electromagnetic radiation of the source, i.e., preventing EMC attack, minimizing the victim's exposure to the attack, and creating immunity of the victim to electromagnetic waves. Thus, the goal of EMC can be described as the correct operation of different equipment in a common electromagnetic environment [11]. In this manner, most of the countries, regions and unions determine their own EMC standards, and test methods. For a firm to be able to sell induction heating systems commercially, EMC filter circuitry must be used to comply to the standards.

Invertor is the third part of the power electronics circuit. Inverters are electronic circuits used to convert direct current to an alternating with constant or variable amplitude and frequency [21,22]. In case of an induction hob, inverter converts the DC voltage supplied by rectifier to AC voltage by using switching elements (e.g. IGBTs) to adjust the voltage and frequency to suitable values for meeting desired efficiency [17]. Induction hobs operate commonly in a frequency range extending from 20 kHz to 40 kHz [24]. This range is usually preferred to achieve maximum efficiency and to avoid noise while heating a pan [25].

The control circuit of an induction heating system, on the other hand, manages the operation of the system and its parts by means of a microcontroller and other peripherals on it [26,27]. Control circuit in an electrical circuit of an induction hob is seen in right part in Figure 1.2.1.1. As seen, control circuitry consists of microcontroller unit (MCU), IGBT gate driver, buzzer, fan control, etc. The first responsibility of the control circuit is to measure grid voltage and frequency to check if they are in suitable ranges. In addition, control circuit detects if there is any material in the magnetic field created by coil by measuring the current flowing through the coil [28]. Upon the detection of a material, control circuit enables switching elements in inverter section to supply alternating current to the coil [18]. If there is no material in magnetic field then control circuit stops supplying a current to the coil to increase efficiency. Furthermore, to maintain induction heating system to operate safely, control circuit keeps monitoring temperature of heating elements with the help of thermistors [29]. Photograph of an electronic card on which power and

control circuits of a commercially available induction heating system exist is represented in Figure 1.2.1.2.

Figure 1.2.1.2 Power electronics and control circuit of an induction hob [30].

1.2.2 Coils

Another important part of the induction heating systems is coils. When a direct current is applied to a coil, it produces a constant magnetic field, and when alternating current is applied, it produces a varying magnetic field [31]. With the help of the inverter circuit, in an induction heating system an alternating current flow on the coil. Thus, coil produces varying magnetic field around it. If a conducting material is placed close to the coil, thanks to varying magnetic field, eddy currents are created on the conducting material. Because the material has a finite conductivity and self-resistance, it starts to be heated up. Since coil is a part of induction heating system, where electrical energy is converted to magnetic energy, its properties such as material conductivity, wire radius, rounding diameter, and shape play important roles on the overall system efficiency [31,32].

There are various coil architectures reported in literature. Since induction hobs enable heating on its surface, planar coils are used in them. Different planar coil structures

presented in literature works and exist in commercially available induction hobs are shown in Figure 1.2.2.1 [33,34].

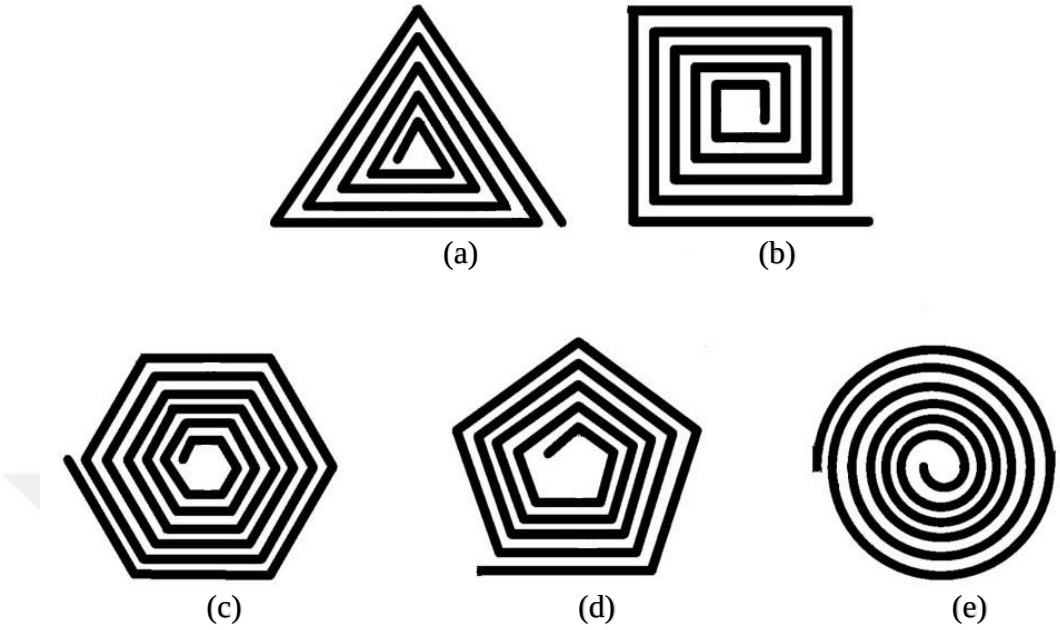

Figure 1.2.2.1 Different planar coil architectures such as (a) triangle, (b) square, (c) pentagon, (d) hexagon, (e) circle used for induction heating systems [35].

Because of their sharp corners production of square-like shaped and triangular-like shaped coils is not as easy as production of circular shaped coils [36,37]. Although advanced production techniques are used, it is inevitable to see some amount of rounding at a corner of coils that have sharp corners. In addition to manufacturing difficulties, in some designs rounded corners of coils that have sharp corners are willingly obtained. In literature there are studies in which squircle coils are reported [38-40]. In these studies, an array of squircle coils is proposed to be used in all-surface induction hobs for complete user flexibility. In addition, it is claimed that in all-surface induction hobs efficiency can be enhanced by phase difference application. For square lattice alignment of coils because of its easiness 180° phase difference is applied between currents of neighbor coils. Also, constructive interaction between neighbor coils is observed when 180° phase difference exists between the coil currents. On the other hand, 0° phase difference exists for the proposed systems between current of diagonally located coils in the square lattice alignment. On the contrary of constructive interaction between neighbor coils, because of in-phase currents destructive field interactions are observed between diagonally located coils. To increase constructive field interactions between neighbor coils and to decrease destructive field interactions between cross coils, squircle coils that have long tangential

sides and rounded corners have been proposed in literature [41]. An array of squircle coils aligned in a square lattice is represented in Figure 1.2.2.2. As seen, 180° phase difference exists between the neighbor coil currents. Therefore, in the figure, currents are shown to flow in the opposite directions for the neighbor coils and in the same direction for the cross coils.

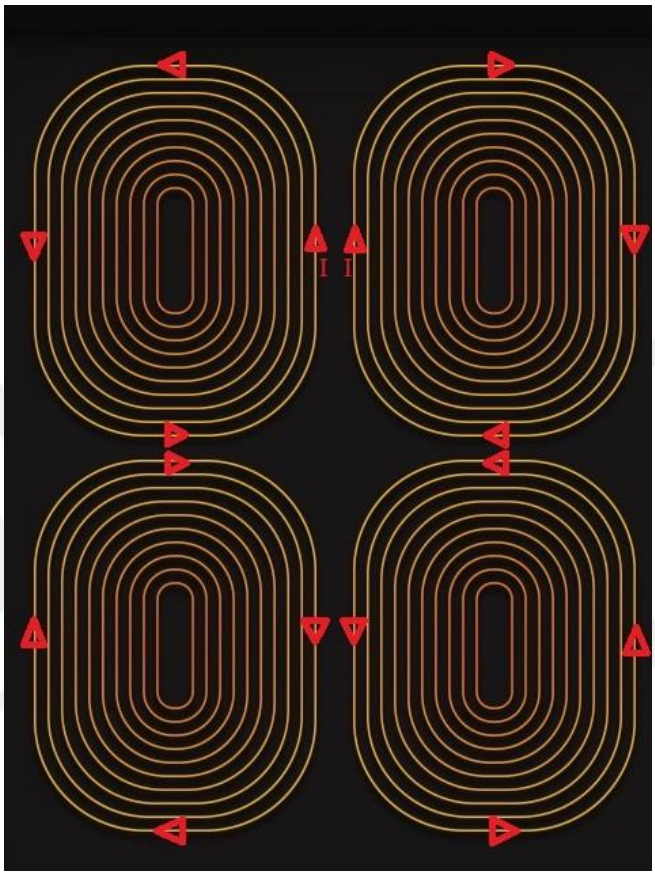

Figure 1.2.2.2 An array of squircle coils aligned in a square lattice, where 180° phase difference exists between neighbor coil currents.

In short, it is very difficult to produce coils having sharp corners. Therefore, at production stage coils that were designed to have sharp corners are manufactured to have rounded corners. In addition, in some systems it is desired that the coils have rounded corners. The change in the coil geometry by rounding its corners affects magnetic field created by the coil and so the coil inductance.

There are formulas in literature to calculate magnetic fields and magnetic flux created by regular shaped coils. As an example, square and circular shaped coils are illustrated in Figure 1.2.2.3 and magnetic flux created by these coils is formulated in (1.2.2.1) and (1.2.2.2), respectively [41].

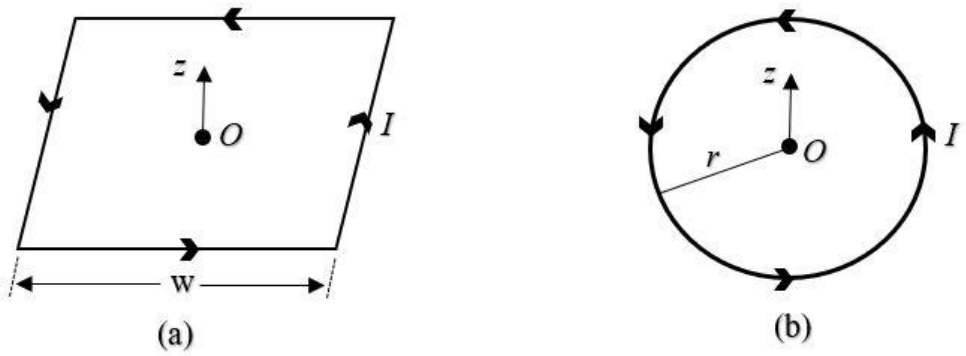

Figure 1.2.2.3 Coils with regular shapes: (a) square coil, (b) circular shaped coil.

$$\vec{B} = \hat{a}_z \frac{2\sqrt{2}\mu_0 I}{\pi w} \quad \textbf{(1.2.2.1)}$$

$$\vec{B} = \hat{a}_z \frac{\mu_0 I}{2b} \quad \textbf{(1.2.2.2)}$$

In the equations μ_0 is the magnetic permeability of free space and I is the current flowing on the coil. On the other hand, in (1.2.2.2) b represents radius of the circular coil shape. Similarly, in (1.2.2.1) w stands for side length of the square coil. As seen, magnetic flux is in $\vec{z}$ direction for both geometries.

Although there are formulas to calculate magnetic field created by regular shaped coils and squircle coils were examined experimentally before, there is no study in literature that analytically examines coils with rounded corners. In this thesis, to fill this gap we analytically investigated planar coil architectures having rounded corners and we derived a formula to calculate magnetic field created by the coils. The derivations were obtained for squircle coils and triangular coils with rounded corners. After derivation, we calculated magnetic flux densities created by the coils at the center for the coils having different sizes and different amounts of rounding. These calculations were repeated for two different cases. In the first case, since rounded corners are indeed arcs of circles, we assumed that the four arcs at the corners are parts of the same circle and center of this circle, is selected to be coinciding with the center of the coil. We calculated magnetic field density at the center of these coils by using our derived formula and the formula exists in literature. We compared the results and checked accuracy of the derived formula. In the second case, on the other hand, corners of the coils are rounded such that the arcs at the corners are parts of circles positioned at different locations. Therefore, centers of the circles containing these arcs at the corners do not coincide with the center of the coil. In our analysis we selected the coils to have side lengths similar to side lengths of

commercially available pans used in induction heating. For fair comparison, we repeated our analysis both for coils having different side lengths and for coils having constant total length but different amounts of rounding. Since the formulas exist in literature are only for regular shaped coils, it is not possible to calculate magnetic flux densities at the center of a coil in our second case with the formulas exist in literature. Therefore, in the second case, we calculated magnetic flux densities only with our derived formulas. However, we simulated all the coils, i.e., both squircle and triangular shaped coils, that we analytically investigated by using a three-dimensional (3D) electromagnetic (EM) solver. The calculated results and the results obtained with simulations match very well.

Before explaining derivation of mentioned formulas, a brief information will be given about induction system usage areas where either planar and non-planar coils are preferred depending on the application.

1.3 Induction System Applications in Different Areas

In addition to heating, induction systems have usage in various areas. One of the applications where induction technology is used is metal detection. Metal detector systems are based on electromagnetic induction technology operating at low frequencies (10 Hz - 100 kHz) [42]. These devices, which are available in fixed or portable models, are intended to detect valuable or dangerous buried (or covered) metal objects. While fixed metal detectors are mostly used in crowded places such as airport, shopping mall, etc. for security purposes, portable detectors are used for various purposes such as mine search, archaeological surveys and gold hunting [43]. A simple metal detector system consists of three main parts that are “data acquisition and control system”, “pulse transmitter and transmitter coil”, and “receiver and receiver coil” as shown in figure 1.3.1.

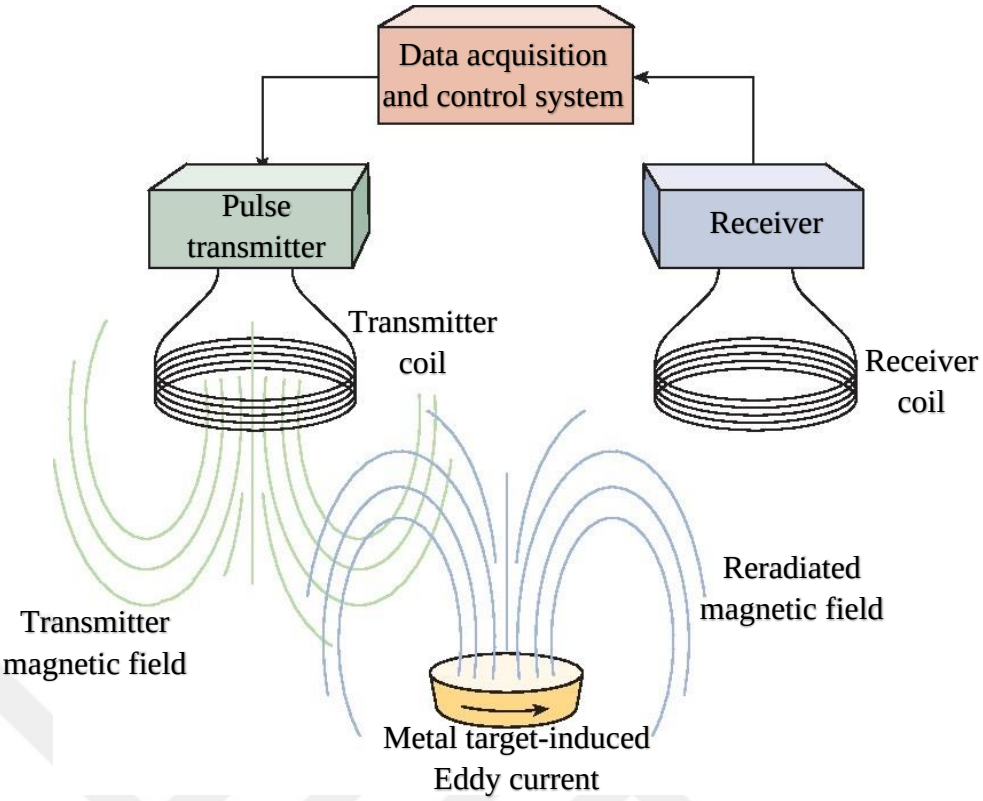

Figure 1.3.1 Exemplary metal detection system model [44].

Another induction system application is metal melting. Melting is the event of dissolving a solid by ionizing it in a liquid. In other words, melting can be defined as the transition from solid phase to liquid phase as a result of heating of a material and turning into liquid phase by breaking the intermolecular bond [45]. There are different methods for metal melting. Because of the advantages of electricity such as being easy to convert to other types of energy, being easy to produce, does not harm the environment like other fossil fuels, and being obtained from various sources; induction technology that uses electrical energy as its source is widely used for metal melting. Induction heating is a non-contact heating method used to heat metallic particles to specified temperatures in a short duration. The tendency to induction furnaces in which metals are melted has increased due to reasons such as ease of control, high efficiency, extremely low material losses, suitability for fully automatic production and no environmental pollution [46]. For metal melting usually multiturn coils are used as shown in figure 1.3.2.

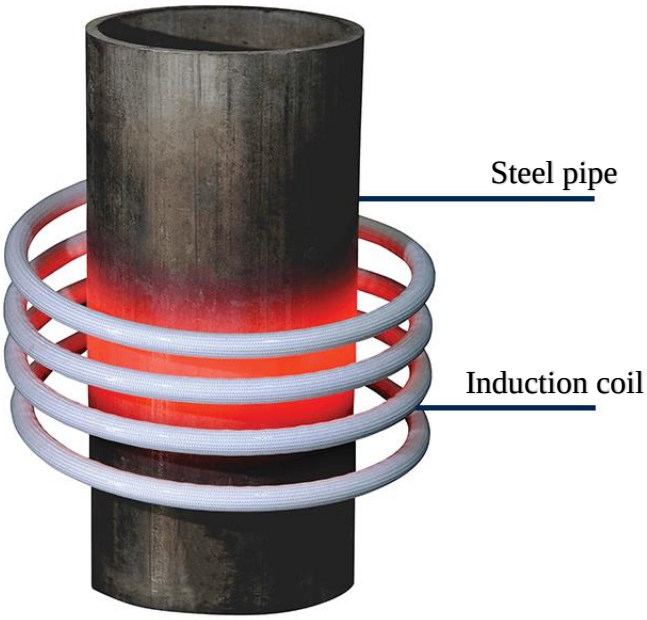

Figure 1.3.2 Exemplary multiturn coil used for metal melting [47].

The next area that induction systems are used is wireless power transmission. The wireless energy transfer adventure, which started with Tesla, has gradually increased its importance as technology has become a multidisciplinary field and has become a common field of study of different disciplines [48]. Today with the development of technology and production of new devices such as cell phones, electrical cars, and so on, providing flexibility to the customers becomes one of the important concerns. Resultantly, in today's world it turns out to be necessary to overcome dependence of users to wire connections that are generally used for charging purpose. To overcome this problem inductively coupled systems are proposed and developed. As an example, cell phones with wireless charging feature are commercially available today. Also, there are studies about wireless charging of electrical cars. Exemplary wireless power transfer system structure is illustrated in figure 1.3.3.

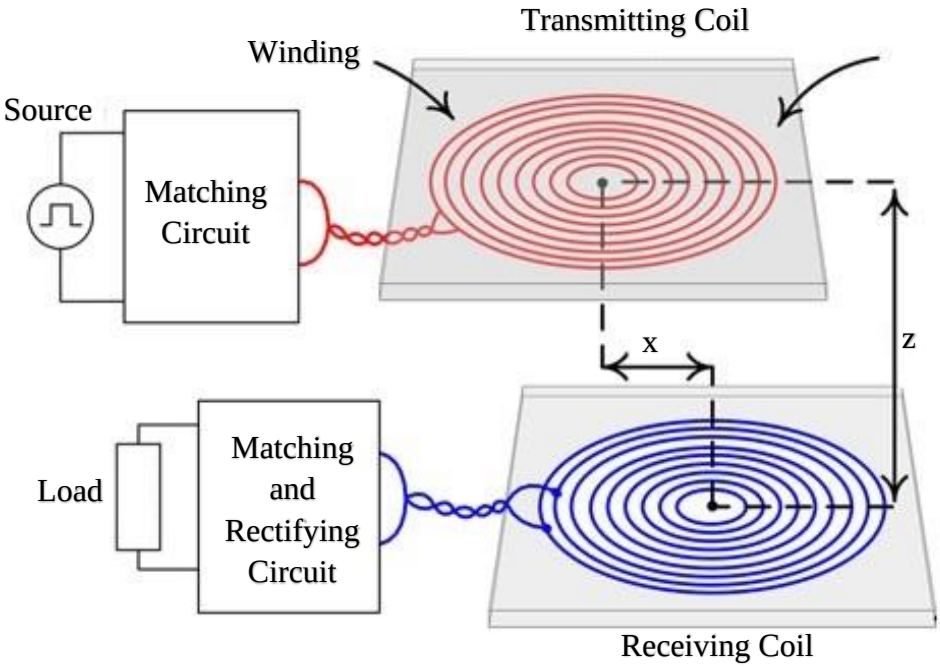

Figure 1.3.3 Exemplary wireless power transfer system structure [49].

Chapter 2

Investigation of Squircle Coils

As it is mentioned in the introduction section, while producing coils that have sharp corners, it is inevitable to have some amount of rounding at the corners. Similarly, there are studies in which coils with rounded corners are proposed to be used in induction heating systems. In a system design, coil inductance and resistance values are important parameters. Inductance of a coil determines resonance frequency and imaginary part of input and output impedances. Therefore, knowing coil parameters and adjusting them to be equal to desired values are crucial for setting system resonance frequency and obtaining good impedance match. Since inductance of a coil is determined by integral of magnetic flux density produced by the coil, it is necessary to calculate magnetic flux density in a coil design. Relation between self-inductance of a coil and magnetic flux density produced by that coil together with current flow on it is given in equation (2.1). Here *L* is the self-inductance of the coil, $\vec{B}$ is magnetic flux density generated by the coil, $d\vec{S}$ is a unit area such that the surface S area over which integral is calculated is limited by current path, i.e., coil wire turn, and I is the current flowing on the coil wire.

$$L = \frac{\int \vec{B}.d\vec{S}}{I} \tag{2.1}$$

Formulas of magnetic field and magnetic flux density created by a straight wire and a wire turn are well-known. Planar coils exist in traditional induction hobs have circular and square type shapes. Since coils with these regular shapes only consist of straight wires or wire turns, magnetic field and magnetic flux density created by these coils are formulated in literature. In the introduction section formulas of magnetic flux density generated by a circular and a square coil are given in equations (1.2.2.2) and (1.2.2.1), respectively. On the other hand, in literature there is no formula to calculate magnetic field created by the rounded corners of a coil. In this chapter, to fill this gap we

analytically examined rounding of corners in a square shaped coil. Contribution of the rounded corners in square shaped coils is formulated and for various coil sizes magnetic flux densities generated by the coil at its center are calculated.

2.1 Squircle Coil Geometry

Square shape with rounded corners is illustrated in Figure 2.1.1. This structure has a special name “squircle”. As can be understood from its name, squircle shape is a combination of or an intermediate between a square and a circle.

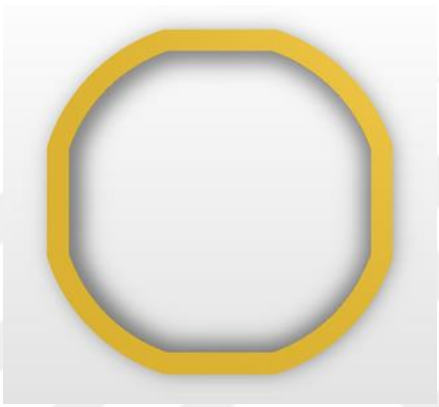

Figure 2.1.1 Square shape with rounded corners (squircle geometry).

As seen in the figure, squircle shape has flat edges and rounded corners that meet at joint points. To be able to calculate overall magnetic field created by squircle shape at the center, it is required to determine contribution of edges and corners separately. Because formula of magnetic field generated by a straight wire is already known and given in the introduction section, it is used to calculate contribution of edges. On the other hand, to calculate contribution of the corners to the overall magnetic field created by the squircle shape coil at its center we first investigated the geometry and obtained geometrical derivations for the corners.

Part of a squircle coil geometry is shown in Figure 2.1.2 together with the assigned geometrical parameters.

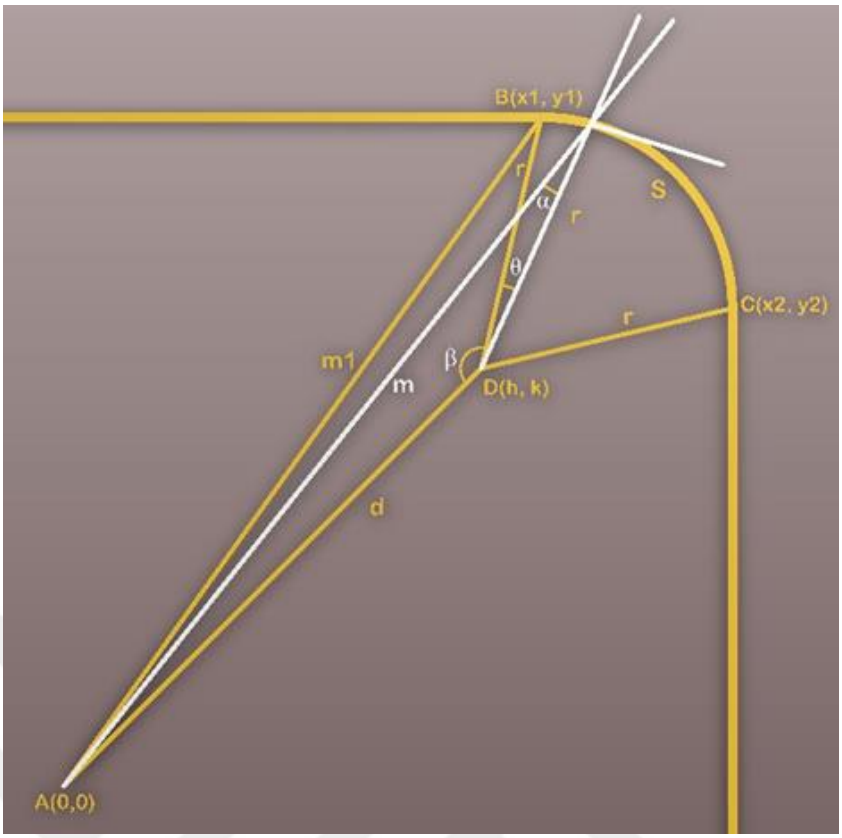

Figure 2.1.2 Part of a squircle coil geometry together with the geometrical parameters.

In the figure, the point A(0,0) represents the center of squircle shape and accepted as reference point for further steps. Points B(x_1,y_1) and C(x_2,y_2), on the other hand, stand for start and end points of the arc, respectively. Similarly, point D(h,k) represents the center point of the arc. Here, rounding corner is assumed to be a part of circle that passes through the points B and C. Since the arc is concave, center of the circle containing the arc is located to be at the inner side of the squircle geometry. In addition, in the figure the length between the points A-B and A-D are labeled as *m1* and *d*, respectively. Radius of the circle that contains the arc is pointed out with label *r* and arc length is labeled with *S*. Also, in the figure angles α, β, and θ are illustrated, too. Here, α is the angle between the two lines where the first line connects the point A and the selected arbitrary point on the arc; and the second line connects the point D and the selected point on the arc. Length of the first line is represented with *m* in the figure. β is another angle between the lines connecting the points A-D and B-D. θ, on the other hand, is the third angle that is between the lines connecting points B-D; and D and selected point on the arc. These assigned geometrical parameters are used in our derivations explained below.

2.2 Magnetic Flux Density Formula Derivations

In our derivations, we initially calculated the distance *m1* between the center of the squircle geometry A(0,0) and start point of the arc B(x_1,y_1). The relation is given in equation (2.2.1).

$$m_1=\sqrt{x_1^2+y_1^2} \tag{2.2.1}$$

By using triangle rule, we can define *m1* as functions of arc radius *r* and the distance between the center of the squircle geometry and the arc center *d*, together with angle *β* between *d* and line that passes from points D(h, k) and B(x_1, y_1). The relation is written in (2.2.2), where cosine of angle β is left alone.

$$\cos(\beta)=\frac{r^2+d^2-m_1^{\,2}}{2rd} \tag{2.2.2}$$

Similarly, relation between parameters (*β*+*θ*), *r*, *d*, and *m* in Figure 2.1.2 can be found as in equation (2.2.3).

$$\cos(\beta+\theta)=\frac{r^2+d^2-m^2}{2rd} \tag{2.2.3}$$

The cosine term in equation (2.2.3) is expanded as functions of sines and cosines of angles *β* and *θ*. Cosine of angle *β* is formulated in (2.2.2). We put this equation into other equations as shown below.

$$\sin(\beta)=\sqrt{1-\cos^2(\beta)} \tag{2.2.4}$$

$$\sin(\beta)=\sqrt{1-\left[\frac{r^2+d^2-m_1^{\,2}}{2rd}\right]^2} \tag{2.2.5}$$

$$\cos(\beta+\theta)=\cos(\beta).\cos(\theta)-\sin(\beta).\sin(\theta) \tag{2.2.6}$$

Equation (2.2.4) is a known trigonometric formula, and by placing equation (2.2.2) into equation (2.2.4), equation (2.2.5) is found. Similarly, equation (2.2.6) is another trigonometric formula and if we place equations (2.2.2), (2.2.3), and (2.2.5) into equation (2.2.6), equation (2.2.7) is derived.

$$\frac{r^2+d^2-m^2}{2rd}=\frac{r^2+d^2-m_1^{\,2}}{2rd}\cos(\theta)-\sqrt{1-\left[\frac{r^2+d^2-m_1^{\,2}}{2rd}\right]^2}\sin(\theta) \tag{2.2.7}$$

By leaving *m* alone in left hand side of equation (2.2.7), equation (2.2.8) is obtained.

$$m=\sqrt{-(r^2+d^2-m_1^2)\cos(\theta)+2rd\sqrt{1-\left[\frac{r^2+d^2-m_1^2}{2rd}\right]^2}\sin(\theta)+r^2+d^2} \quad \textbf{(2.2.8)}$$

In the equation *r*, *d*, and m_1 are constants but *m* and θ are variables that change with position of selected point on the arc.

In calculation of magnetic flux density contribution of the arc, effect of each point on the arc to the total magnetic flux density needs to be taken into account. This is achieved in Biot-Savart rule by taking integral over the contour on which current is flowing. The Biot-Savart rule that is used to calculate generated magnetic flux density by a current I flowing on contour C is given in equation (2.2.9).

$$\vec{B} = \frac{\mu_0}{4\pi}\oint_C I\frac{d\vec{l}x\hat{r}}{|r|^2} \quad \textbf{(2.2.9)}$$

In the equation (2.2.9), μ_0 stands for permeability of free space, *dl* represents selected infinitely small length on the arc, and *r* is radius of the arc. If we apply Biot-Savart rule to calculate magnetic flux density distribution of the arc in the part of squircle coil geometry that is shown in Figure 2.1.2, then the following equation is obtained, where θ_1 is the maximum central angle of the arc, i.e., the angle between $B(x_1, y_1)$ - D(h, k) and $C(x_2, y_2)$ - D(h, k) lines.

$$B = \frac{u_0 I}{4\pi}\int_0^{\theta_1}\frac{r\cos(\alpha)}{m^2}d\theta \quad \textbf{(2.2.10)}$$

In the equation μ_0, *I*, *r*, and θ_1 are known parameters. Therefore, to calculate the integral *m* and $\cos(\alpha)$ should be written as functions of θ. From the geometrical triangle rule $\cos(\alpha)$ can be written as a function of known parameters and *m* as shown in equations (2.2.11) and (2.2.12).

$$d^2 = m^2 + r^2 - 2mr\cos(\alpha) \quad \textbf{(2.2.11)}$$

$$\cos(\alpha) = \frac{m^2 + r^2 - d^2}{2mr} \quad \textbf{(2.2.12)}$$

If we put equation (2.2.12) into equation (2.2.10), the following equation is obtained.

$$B = \frac{u_0 I}{8\pi}\int_0^{\theta_1}\frac{m^2 + r^2 - d^2}{m^3}d\theta \quad \textbf{(2.2.13)}$$

Equations (2.2.8) and (2.2.13) are the general formulas that we derived to calculate magnetic flux contribution of an arc in a squircle coil. In equation (2.2.13) except *m*, all

the other parameters are constant such that their values depend on squircle coil geometry. On the other hand, m is a function of θ and their relation is given in equation (2.2.8).

2.3 Calculated Magnetic Flux Density Results

After deriving the formulas, we used them to calculate magnetic flux densities generated by squircle shaped coils with three different sizes that are selected among common coil sizes used in industry. Side lengths of the coils are set to be 7.5 cm, 16.0 cm, and 28.0 cm. In addition, for each case, different amounts of rounding are selected to examine effect of the rounding on overall magnetic field of the coil.

Calculations are done for two different cases. In the first case, arcs at the corners are selected to be parts of a circle such that center of the circle (point D(h,k) in Figure 2.1.2)) is selected to be coinciding with the center of the coil (point A(0,0) in Figure 2.1.2). In this geometry since arcs are parts of a circle whose radius and angles corresponding to the arcs can easily be found out from the start and end points of the arcs, contribution of the arcs to magnetic flux density at the center is calculated by applying magnetic flux density formula at the center of a circular coil that is given in equation (1.2.2.2) in the introduction section. In addition, contribution of the straight edges to total magnetic flux density at the coil center is easily calculated from the well-known formulas exist in literature. Resultantly, in case 1 magnetic flux density created by a squircle coil is calculated by using both our proposed method and the traditional method. By this way, it is possible to make a fair comparison between the methods and to calculate the error of our derived formula compared to traditional formula. In the second case, on the other hand, in squircle geometry rounding at the corners is done starting from a square geometry with total length of the coil to be unchanged. This results in four different circles that combine arcs to have centers at different points. Also, centers of the circles that contain the arcs (such as point D(h,k) in Figure 2.1.2) are not coinciding with center of the squircle geometry (point A(0,0) in Figure 2.1.2). Because of the unusual geometry, in the second case magnetic flux density calculations cannot be done by using traditional formulas. Therefore, for the second case we calculated magnetic flux density at the center of coils by using our derived formulas and obtained results were verified by the simulations. The results are given in next chapters.

In both cases, for each coil size and different amount of rounding, there are 4 identical arcs at the corners and they are symmetric to each other with respect to x-axis and y-axis. Similarly, in both geometries, coils have 4 identical symmetric edges. Since arcs and edges are identical for a particular coil, it is enough to calculate magnetic flux density contributions of an edge and an arc and to multiply their sum with 4 to determine overall magnetic flux density created by the coil.

2.3.1 Case 1: Squircle Geometry with Arcs Containing by a Circle whose Center is Coinciding with the Middle Point of the Squircle Geometry

We first obtained calculations for the first case where squircle geometry is set such that arcs at the corners are identical and they are symmetric with respect to coil center. In addition, arcs are parts of the same circle whose center is coinciding with center of the squircle coil geometry. Calculations were repeated for coils having different size lengths and different amounts of rounding. In Figure 2.3.1.1, squircle coil geometry in case 1 having 16 cm side length and different amounts of rounding at its corners is illustrated. As seen, the coil is first designed to have no rounding such that it has a square shape in (a), and then the coil corners are rounded by increasing amounts in (b), (c), and (d), respectively. At the end, if the corners are rounded fully as in subfigure (e) then the coil has a circular geometry. It means, limit of the squircle geometry is approaching to square geometry on one side and to circular geometry on the other side.

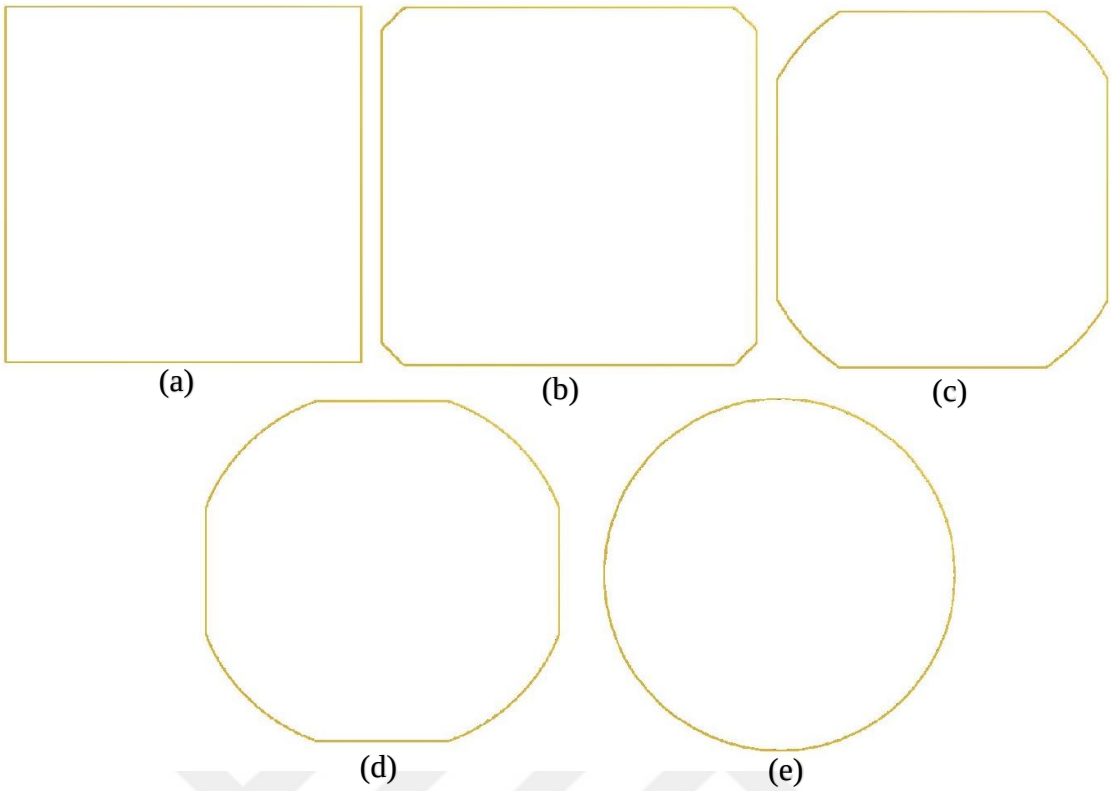

Figure 2.3.1.1 Squircle shaped coils with different amounts of rounding at the corners. Here, side length of the coils is selected to be 7.5 cm and length of the straight parts is (a) 16 cm, (b) 10 cm, (c) 6 cm, (d) 2 cm, (e) 0 cm. In addition, here centers of the circles containing the arcs are selected to be coinciding with the coil center.

Geometrical parameters of squircle shaped coils having different corner roundings investigated in case 1 are given in Table 2.3.1.1, Table 2.3.1.2, and Table 2.3.1.3 for coil side lengths equal to 7.5 cm, 16.0 cm, and 28.0 cm, respectively. In the tables, the parameter named as "Arc Start Point" indicates coordinates of the point at which one of the edges (in Figure 2.1.2 it is the edge at top) of squircle coil ends and arc starts (point B(x_1, y_1) in Figure 2.1.2). Similarly, the second parameter in the tables called "Arc End Point" stands for the point at which the arc ends and the other edge of the coil starts (point C(x_2, y_2) in Figure 2.1.2). On the other hand, the parameters named "Arc Length" and "Edge Length" describe lengths of an arc and an edge, respectively, in unit of cm. Because of the squircle geometry symmetry in case 1, start and end points of the other arcs in the coils can be found very easily. In addition, all the arcs have the same length. The fifth parameter in the tables, i.e., "Arc Radius", corresponds to radius length of the circle that contains the arc (distance *r* in Figure 2.1.2). Since the squircle geometry in case 1 is set such that center of the circle containing the arcs coincide with the center of the squircle geometry and the edges and the arcs in squircle geometry are identical and symmetric with respect to the center, the parameter in the tables named as "Center Coordinates" is

selected as (0, 0). Finally, the last parameter in the table named "Arc Angle" is the central angle of an arc (θ_1 in equation (2.2.10)).

Arc Start Point (cm, cm)	Arc End Point (cm, cm)	Arc Length (cm)	Edge Length (cm)	Arc Radius (cm)	Center Coordinates (cm, cm)	Arc Angle (radian)
(3.75, 3.75)	(3.75, 3.75)	0	3.75	0	-	0
(3.74, 3.75)	(3.75, 3.74)	0.014142	3.74	5.296234	(0, 0)	0.0026702
(2.50, 3.75)	(3.75, 2.50)	1.779299	2.50	4.506939	(0, 0)	0.3947911
(1.25, 3.75)	(3.75, 1.25)	3.665456	1.25	3.952847	(0, 0)	0.9272952
(0, 3.75)	(3.75, 0)	5.890486	0	3.750000	(0, 0)	1.5707963

Table 2.3.1.1 Geometrical parameters of squircle shaped coil with a side length equal to 7.5 cm having different amounts of rounding.

Arc Start Point (cm, cm)	Arc End Point (cm, cm)	Arc Length (cm)	Edge Length (cm)	Arc Radius (cm)	Center Coordinates (cm, cm)	Arc Angle (radian)
(8.00, 8.00)	(8.00, 8.00)	0	8.00	0	-	0
(7.99, 8.00)	(8.00, 7.99)	0.014142	7.99	11.30663	(0, 0)	0.001250
(7.00, 8.00)	(8.00, 7.00)	1.415258	7.00	10.63014	(0, 0)	0.133136
(5.00, 8.00)	(8.00, 5.00)	4.279232	5.00	9.433981	(0, 0)	0.453597
(3.00, 8.00)	(8.00, 3.00)	7.290213	3.00	8.544003	(0, 0)	0.853254
(0, 8.00)	(8.00, 0)	12.56637	0	8	(0, 0)	1.570796

Table 2.3.1.2 Geometrical parameters of squircle shaped coil with a side length equal to 16.0 cm having different amounts of rounding.

Arc Start Point (cm, cm)	Arc End Point (cm, cm)	Arc Length (cm)	Edge Length (cm)	Arc Radius (cm)	Center Coordinates (cm, cm)	Arc Angle (radian)
(14.00, 14.00)	(14.00, 14.00)	0	14.00	0	-	0
(13.99, 14.00)	(14.00, 13.99)	0.014142	13.99	19.79192	(0, 0)	0.000714
(11.00, 14.00)	(14.00, 11.00)	4.252743	11.00	17.80449	(0, 0)	0.238857
(8.00, 14.00)	(14.00, 8.00)	8.586370	8.00	16.12451	(0, 0)	0.532504
(5.00, 14.00)	(14.00, 5.00)	13.15273	5.00	14.86606	(0, 0)	0.884748

(0, 14.00)	(14.00, 0)	21.99114	0	14	(0, 0)	1.570796

Table 2.3.1.3 Geometrical parameters of squircle shaped coil with a side length equal to 28.0 cm having different amounts of rounding

In the tables, it is seen that each coil starts with zero arc length that corresponds to a square shape, and continues with increasing arc length. At the end coils have no edges and they turn into complete circular shaped coils. Increasing arc length allows us to see the effect of rounding in a squircle shape coil to the created magnetic field at the center of the coil.

Calculated magnetic flux densities at the center of squircle coils having different roundings are given in Table 2.3.1.4, Table 2.3.1.5, and Table 2.3.1.6 for side lengths equal to 7.5 cm, 16.0 cm, and 28.0 cm, respectively.

Arc Start Point (cm, cm)	**Magnetic Flux Density Calculated by Proposed Method (Wb/cm^2)**	**Magnetic Flux Density Calculated by Traditional Method (Wb/cm^2)**	**Error Between Proposed and Traditional Methods (%)**
(3.74, 3.75)	1.5087E-05	1.508495 E-05	0.014
(2.50, 3.75)	1.5337E-05	1.533745 E-05	0.003
(1.25, 3.75)	1.6111E-05	1.612976 E-05	0.116
(0, 3.75)	1.6710E-05	1.675516 E-05	0.270

Table 2.3.1.4 Calculated magnetic flux density of squircle shaped coil with a side length equal to 7.5 cm having different amounts of rounding.

Arc Start Point (cm, cm)	**Magnetic Flux Density Calculated by Proposed Method (Wb/cm^2)**	**Magnetic Flux Density Calculated by Traditional Method (Wb/cm^2)**	**Error Between Proposed and Traditional Methods (%)**
(7.99, 8.00)	7.0738E-06	7.071069 E-06	0.039
(7.00, 8.00)	7.0910E-06	7.086022 E-06	0.070
(5.00, 8.00)	7.2253E-06	7.223239 E-06	0.029
(3.00, 8.00)	7.5091E-06	7.505872 E-06	0.043
(0, 8.00)	7.8414E-06	7.853981 E-06	0.160

Table 2.3.1.5 Calculated magnetic flux density of squircle shaped coil with a side length equal to 16.0 cm having different amounts of rounding.

Arc Start Point (cm, cm)	Magnetic Flux Density Calculated by Proposed Method (Wb/cm^2)	Magnetic Flux Density Calculated by Traditional Method (Wb/cm^2)	Error Between Proposed and Traditional Methods (%)
(13.99, 14.00)	4.0412E-06	4.040610 E-06	0.015
(11.00, 14.00)	4.0674E-06	4.067032 E-06	0.009
(8.00, 14.00)	4.1573E-06	4.156059 E-06	0.030
(5.00, 14.00)	4.3032E-06	4.302507 E-06	0.016
(0, 14.00)	4.4886E-06	4.487989 E-06	0.013

Table 2.3.1.6 Calculated magnetic flux density of squircle shaped coil with a side length equal to 28.0 cm having different amounts of rounding.

In the tables, arc start points are given to understand amount of rounding for different sized coils. In addition, total magnetic flux densities at the center of the coils calculated by using the proposed method and the traditional method are given in the tables. As we described before, since in this case center of the circle containing the arcs are selected to be coinciding with the center of the coil, it is possible to calculate magnetic flux densities at the center by using the proposed and the traditional methods, thus it is possible to compare these two methods fairly. We also calculated the error between two results and shared in the tables in percentages. As seen in the tables, the maximum error is found to be 0.27 %. The low error rate demonstrates the correctness of formulas that we derived in this study.

2.3.2 Case 2: Squircle Geometry with Arcs Containing by Different Circles whose Centers are not Coinciding with the Middle Point of the Squircle Geometry

After proving validity and correctness of the derived formula for the squircle coil geometry in the first case, in the second case magnetic flux density created by coils having squircle geometry in which arcs at the corners are parts of different circles such that center points of these circles do not coincide with the middle point of the squircle geometry is formulated. However, as in the previous case, in the second case arcs at the corners are assumed to be identical and symmetric with respect to x and y-axis.

In the second case, magnetic flux densities created at the center of the coils are investigated for different squircle coil geometries. As in previous case, rounding of the

corners is changed. However, for fair comparison, total length of coils is kept constant (in the first case, side length of the coils was kept constant). By this way, it is possible to see effects of rounding to magnetic flux density created at the coil center. In Figure 2.3.2.1, squircle shaped coils with different amounts of rounding at the corners are illustrated. Coils represented in the figure have constant total length equal to 64 cm. Also, center of the coils are set to be at (0, 0) point, thus start points of the arcs at right top are (7 cm, 8 cm), (5 cm, 8 cm), (3 cm, 8 cm), and (0 cm, 8 cm) in subfigures (a), (b), (c), and (d), respectively.

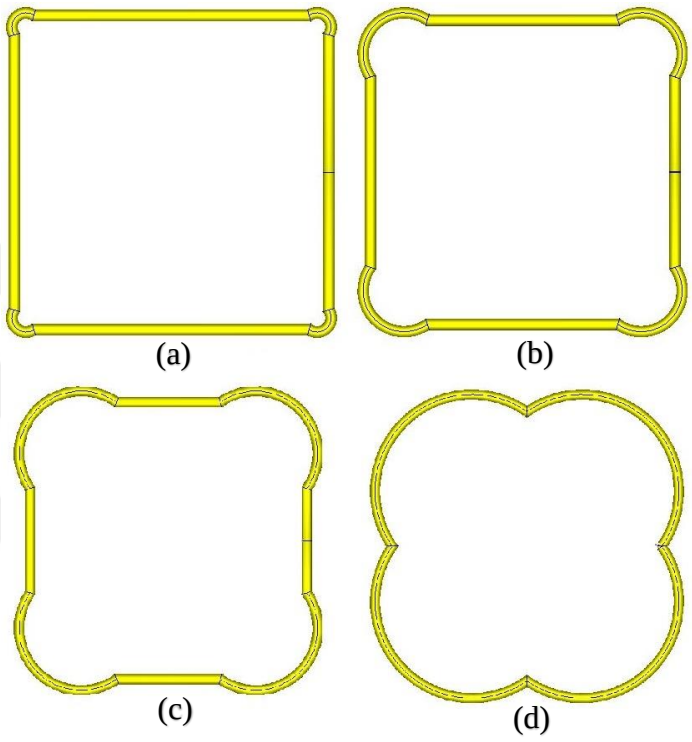

Figure 2.3.2.1 Squircle shaped coils with different amounts of rounding at the corners. Here, total length of the coils is selected to be constant 64 cm and length of the straight parts is (a) 14 cm, (b) 10 cm, (c) 6 cm, and (d) 0 cm. In addition, here centers of the circles containing the arcs are selected to be not coinciding with the coil center.

Before calculating magnetic flux density created by these coils, it is required to find out the geometrical parameters of the coils, i.e., center point, radius, and central angle of circles containing arcs. Derivations of these parameters are described below. Since arcs are identical and they are symmetric with respect to coil center, we obtained derivations and calculations only for a single arc. Total contribution of the arcs to magnetic flux density at the coil center is calculated by multiplying contribution of a single arc with 4.

We began our derivations with an arc that is part of a circle. In Figure 2.3.2.2 an arc that is part of a circle is shown together with its geometrical parameters.

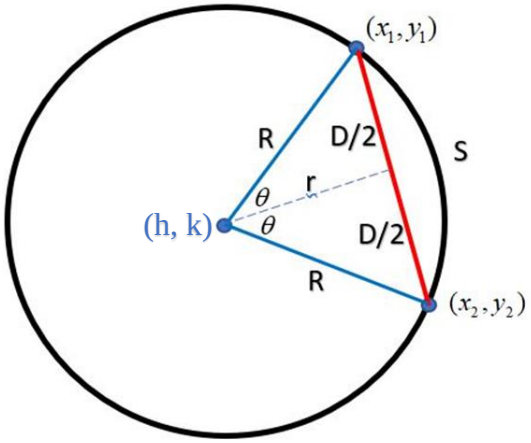

Figure 2.3.2.2 An arc that is part of a circle together with its geometrical parameters.

In the geometry, arc length *S*, and start (x_1, y_1) and end points (x_2, y_2) of the arc are known. Radius of the coil *R* is calculated as a function of known parameters by using following steps. First let's start by writing

$$S = R * 2\theta \tag{2.3.2.1}$$

where θ is in radian. Here, *R* and θ are unknown. If we write θ as functions of known parameters and *R* then we can derive *R* as a function of only known parameters. Below lines are for writing θ as functions of known parameters and *R*.

$$\sin(2\theta) = 2 * \sin(\theta) * \cos(\theta) \tag{2.3.2.2}$$

where

$$\sin(\theta) = \frac{D}{2R} \tag{2.3.2.3}$$

and

$$\cos(\theta) = \frac{\sqrt{R^2 - \frac{D^2}{4}}}{R} \tag{2.3.2.4}$$

By placing equations (2.3.2.3) and (2.3.2.4) into equation (2.3.2.2), we get equation (2.3.2.5).

$$2\theta = \sin^{-1}\left(\frac{D * \sqrt{R^2 - \frac{D^2}{4}}}{R^2}\right) \tag{2.3.2.5}$$

If equation (2.3.2.5) is placed into equation (2.3.2.1), the following equation is obtained to calculate radius *R* of the circle containing the arc.

$$S = \sin^{-1}\left(\frac{D * \sqrt{R^2 - \frac{D^2}{4}}}{R^2}\right) * R \qquad \textbf{(2.3.2.6)}$$

Since in our designs in case 2 total length of a coil is set to be constant, i.e., it does not change with rounding, arc length *S* is known. Also, distance *D* between start and end points of the arc can be calculated, too, by using coordinates of start and end points of the arc. However, equation (2.3.2.6) is so complicated, and it is not easy to solve this equation, i.e. finding roots of the equation, with hand calculations. Therefore, we applied another approach to solve the equation and find arc parameters. By using a mathematical tool Matlab, we iteratively solved the equation (2.3.2.6) for *R* values starting from 0 till a value at which calculated *S* value (right hand side of the equation) is equal to or very close to its real value with an increment of 0.00001 cm. The accuracy of the results can be increased further if an increment lower than 0.00001 cm is used. However, in our cases accuracy of the calculated results are found to be sufficiently good. After finding radius of the circle *R*, center coordinates of the arc are found with the following equations

$$h = x_3 - \sqrt{R^2 - \left(\frac{D}{2}\right)^2} * \frac{y_1 - y_2}{D} \qquad \textbf{(2.3.2.7)}$$

$$k = y_3 - \sqrt{R^2 - \left(\frac{D}{2}\right)^2} * \frac{x_2 - x_1}{D} \qquad \textbf{(2.3.2.8)}$$

where *h* and *k* represent coordinates of the center point of the circle containing the arc. Also, new variables x_3 and y_3 indicate coordinates of the middle point between start and end points of the arc. The variables x_3 and y_3 are calculated with the following formulas.

$$x_3 = (x_1 + x_2) / 2 \qquad \textbf{(2.3.2.11)}$$

$$y_3 = (y_1 + y_2) / 2 \qquad \textbf{(2.3.2.12)}$$

Geometrical parameters of squircle shaped coils having different corner roundings investigated in case 2 are given in Table 2.3.2.1, Table 2.3.2.2, and Table 2.3.2.3 for coil total side lengths equal to 30 cm, 64 cm, and 112 cm, respectively.

Arc Start Point (cm, cm)	Arc End Point (cm, cm)	Arc Length (cm)	Found Arc Length (cm)	Found Arc Radius r (cm)	Found Center Coordinates (cm, cm)
(3.75, 3.75)	(3.75, 3.75)	0	-	-	-
(3.74, 3.75)	(3.75, 3.74)	0.02	0.019968	0.00719	(3.744079103697, 3.7440791036974)
(2.50, 3.75)	(3.75, 2.50)	2.50	2.500034	0.89827	(3.011776784845, 3.0117767848451)
(1.25, 3.75)	(3.75, 1.25)	5.00	4.999985	1.79655	(2.273513904952, 2.2735139049522)
(0, 3.75)	(3.75, 0)	7.50	7.500019	2.69482	(1.535290688676, 1.5352906886763)

Table 2.3.2.1 Geometrical parameters of squircle shaped coil with a total length equal to 30 cm having different amounts of rounding.

Arc Start Point (cm, cm)	Arc End Point (cm, cm)	Arc Length (cm)	Found Arc Length (cm)	Found Arc Radius r (cm)	Found Center Coordinates (cm, cm)
(8.00, 8.00)	(8.00, 8.00)	0	-	-	-
(7.99, 8.00)	(8.00, 7.99)	0.02	0.019968	0.00719	(7.994079103697, 7.9940791036974)
(7.00, 8.00)	(8.00, 7.00)	2.00	1.999994	0.71862	(7.409405561980, 7.4094055619808)
(5.00, 8.00)	(8.00, 5.00)	6.00	5.999982	2.15586	(6.228216685942, 6.2282166859426)
(3.00, 8.00)	(8.00, 3.00)	10.00	9.999971	3.5931	(5.047027809904, 5.0470278099044)
(0, 8.00)	(8.00, 0)	16.00	16.00003	5.74895	(3.275284158273, 3.2752841582730)

Table 2.3.2.2 Geometrical parameters of squircle shaped coil with a total length equal to 64 cm having different amounts of rounding.

Arc Start Point (cm, cm)	Arc End Point (cm, cm)	Arc Length (cm)	Found Arc Length (cm)	Found Arc Radius r (cm)	Found Center Coordinates (cm, cm)
(14.00, 14.00)	(14.00, 14.00)	0	-	-	-
(13.99, 14.00)	(14.00, 13.99)	0.02	0.019968	0.00719	(13.99407910369, 13.994079103697)
(11.00, 14.00)	(14.00, 11.00)	6.00	5.999982	2.15586	(12.22821668594, 12.228216685942)
(8.00, 14.00)	(14.00, 8.00)	12.00	11.99996	4.31172	(10.45643337188, 10.456433371885)
(5.00, 14.00)	(14.00, 5.00)	18.00	18.00003	6.46757	(8.684689720137, 8.6846897201371)
(0, 14.00)	(14.00, 0)	28.00	28.00000	10.0606	(5.731717529707, 5.7317175297079)

Table 2.3.2.3 Geometrical parameters of squircle shaped coil with a total length equal to 112 cm having different amounts of rounding.

In the tables, as in previous case, parameters in the first and the second columns named "Arc Start Point" and "Arc End Point" indicate start and end point coordinates of the arc, respectively. Also, parameters in the third column named as "Arc Length" stand for length of the arc that is known. On the other hand, data in the fourth, fifth, and sixth columns named as "Found Arc Length", "Found Arc Radius r", and "Found Center Coordinates" represent arc lengths, radius of circles containing arcs, and center coordinates of the circle, respectively, found by iteratively solving derived formulas. As seen in the tables, calculated arc lengths are almost the same with the real arc lengths. In addition, found center coordinates in the last column of the tables are different from (0, 0). It means that the center of the circles containing the arcs do not coincide with the center of the squircle shaped coils. Therefore, in the second case it is not possible to use traditional formulas to calculate magnetic flux density created by these coils. However, by using our derived formulas that are given in Chapter 2 we calculated magnetic flux densities at the center of squircle coils having different roundings. Magnetic flux densities at the center of squircle shaped coils in case 2 are given in Table 2.3.2.4, Table 2.3.2.5, and Table 2.3.2.6 for coil total lengths equal to 30 cm, 64 cm, and 112 cm, respectively.

Arc start Point (cm, cm)	**Magnetic Flux Density Created by Edges (Wb/cm^2)**	**Magnetic Flux Density Created by Arcs Calculated by Using Proposed Formula (Wb/cm^2)**	**Overall Magnetic Flux Density Created by Coil (Wb/cm^2)**
(3.74, 3.75)	1.51E-05	2.02E-08	1.51E-05
(2.50, 3.75)	1.18E-05	3.18E-06	1.50E-05
(1.25, 3.75)	6.75E-08	7.97E-06	1.47E-05
(0, 3.75)	0.00E+00	1.41E-05	1.41E-05

Table 2.3.2.4 Calculated magnetic flux density and its contributors in squircle shaped coils with a total length equal to 30 cm and having different amounts of rounding.

Arc start Point (cm, cm)	**Magnetic Field Created by Edges (Wb/cm^2)**	**Magnetic Flux Density Created by Arcs Calculated by Using Proposed Formula (Wb/cm^2)**	**Overall Magnetic Field Created by Coil (Wb/cm^2)**
(7.99, 8.00)	7.07E-06	4.42E-09	7.07E-06
(7.00, 8.00)	6.59E-06	4.82E-07	7.07E-06
(5.00, 8.00)	5.30E-06	1.73E-06	7.03E-06
(3.00, 8.00)	3.51E-06	3.41E-06	6.92E-06
(0, 8.00)	0.00E+00	6.61E-06	6.61E-06

Table 2.3.2.5 Calculated magnetic flux density and its contributors in squircle shaped coils with a total length equal to 64 cm and having different amounts of rounding.

Arc start Point (cm, cm)	**Magnetic Field Created by Edges (Wb/cm^2)**	**Magnetic Flux Density Created by Arcs Calculated by Using Proposed Formula (Wb/cm^2)**	**Overall Magnetic Field Created by Coil (Wb/cm^2)**
(13.99, 14.00)	4.04E-06	1.44E-09	4.04E-06
(11.00, 14.00)	3.53E-06	5.03E-07	4.03E-06
(8.00, 14.00)	2.84E-06	1.17E-06	4.01E-06
(5.00, 14.00)	1.92E-06	2.03E-06	3.95E-06
(0, 14.00)	0.00E+00	3.78E-06	3.78E-06

Table 2.3.2.6 Calculated magnetic flux density and its contributors in squircle shaped coils with a total length equal to 112 cm and having different amounts of rounding.

As it is seen in the tables, while rounding increases, contribution of edges to total flux density decreases but contribution of arcs to total flux density increases. This is expected. However, as rounding increases total magnetic flux density at the center of a coil decreases. In addition, in the tables it is also seen that there is significant change in the overall magnetic flux densities with changes in coil total length.

As an example, change of total magnetic flux density calculated at the center of squircle shaped coils having a 112 cm circumferential length with respect to start points on x-axis is shown in Figure 2.3.2.3.

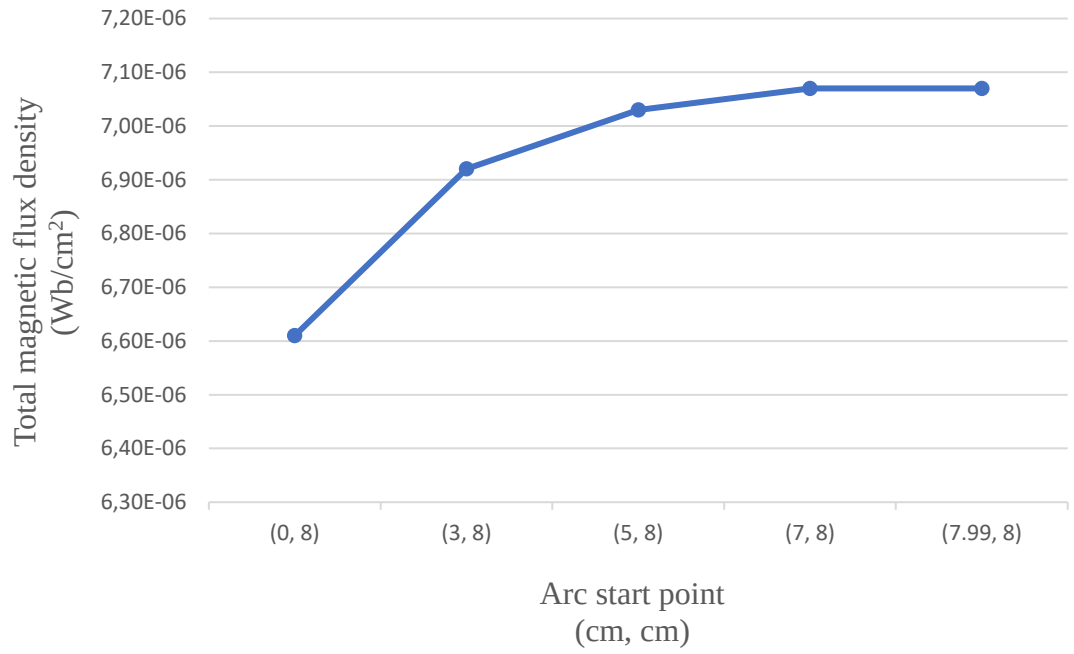

Figure 2.3.2.3 Change of total magnetic flux density calculated at the center of squircle shaped coils having a 112 cm circumferential length with respect to start points on x-axis.

In the figure, the first data that is for (0 cm, 8 cm) arc start point corresponds to fully circular shaped coil with 112 cm circumference. On the other hand, the last data that is for (7.99 cm, 8 cm) corresponds to a squircle shaped coil whose geometry is almost a perfect square shape. As seen in the figure, there is an increasing behavior during transformation of squircle shaped coils starting from circular shaped to square shaped.

Because there is no formulation in the literature to calculate results of the fixed total length case, to check correctness of the found results we obtained electromagnetic simulations of the examined coils. The simulations are described in chapter 4 together with the obtained results.

Chapter 3

Investigation of Triangular Coils

In the previous chapter, proposed formula derivations were done for squircle shaped coils, and correctness of the formula was proved by comparing the results of the magnetic field created at the center of squircle shaped coils calculated by proposed and traditional methods. Although derivations were obtained for squircle shaped coils, they are applicable to any coil shape that has rounded corners. To demonstrate that, in this chapter, the derivations and calculations are repeated for triangular coils. A triangular shape with rounded corners is shown in Figure 3.1.

Figure 3.1 Triangular shape with rounded corners.

Similar to squircle shaped coil, magnetic field calculations were repeated for triangular shaped coils having three different sizes, and for each size different amounts of rounding were considered. Derivations and results are explained and discussed below in detail.

3.1 Magnetic Flux Density Formula Derivations

The variables are selected as symbol while deriving the formula for both squircle and triangular coils. This provides flexibility to apply the same formulation to any shaped of coil. Thus, although centroid of squircle and triangular shapes are at different locations, the same derivations are valid for both geometries. A part of triangular coil structure with geometrical parameters are shown in Figure 3.1.1.

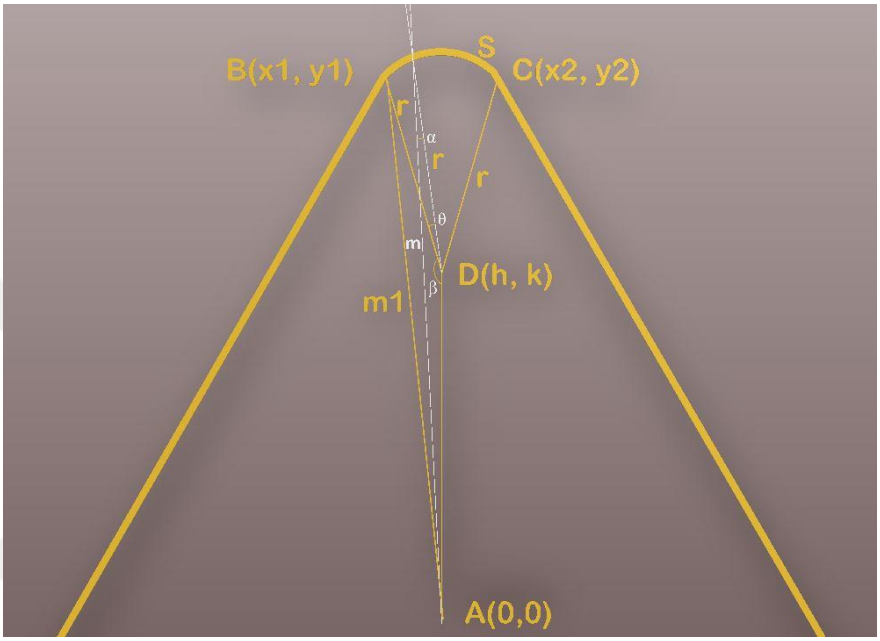

Figure 3.1.1 Part of a triangular coil geometry rounded at its corners together with the geometrical parameters.

In the figure, point A(0, 0) represents the center point of the coil and it is accepted as reference point for further derivations. As in squircle coil geometry (see Figure 2.1.2 in chapter 2), in the figure, points B(x_1, y_1) and C(x_2, y_2) stand for start and end points of the arc, respectively. It is assumed that arcs at the corners those arise due to rounded corners are parts of circles. In the figure, arc at the corner is part of the circle that passes through the points B and C. Since the arc is concave, center of the circle containing the arc that is marked with D(h, k) in the figure is located on the inner side of the coil. Also, in the figure arc length and radius of the arc are labeled as *S* and *r*, respectively. Similarly, distances between points A-B and A-D are labeled as *m1* and *d*, respectively. Since all the geometrical parameters are referenced to center point A(0, 0), magnetic flux density generated by the arc at the center point A(0, 0) is formulated as in equation (3.1.1), which is same with the equation (2.2.13) in chapter 2 derived for the squircle coil geometry.

$$\vec{B}=\frac{u_0 I}{8\pi}\int_0^{\theta_1}\frac{m^2+r^2-d^2}{m^3}d\theta \qquad \textbf{(3.1.1)}$$

Here, μ_0 is the free-space permeability ($4\pi 10^{-7}$ Tm/A) because it is assumed that the coil is located in free-space. Also, *I* corresponds to current intensity flowing on the coil and θ_1 stands for central angle between the lines connecting the points B-D and C-D that sees the arc. As seen in the figure, the parameter *m* in the equation is not constant for points on the arc, i.e., for various θ angles in the integral. Therefore, it is necessary to write *m* as a function of constant geometrical parameters and angle θ. Relation between *m* and other geometrical parameters were derived before in chapter 2 (see equation 2.2.8) and it is rewritten in equation 3.1.2.

$$m=\sqrt{-(r^2+d^2-m_1^{\,2})\cos(\theta)+2rd\sqrt{1-\left[\frac{r^2+d^2-m_1^{\,2}}{2rd}\right]^2}\sin(\theta)+r^2+d^2} \qquad \textbf{(3.1.2)}$$

As seen, *m* is written as a function of constant parameters *r*, *d*, m_1 and angle θ. Parameters *r* and *d* in the equations are defined above. However, the parameter m_1 in the last equation corresponds to distance between the coil center point and start (or end) point of the arc, i.e., distance between the points A-B and A-C.

By using equations (3.1.1) and (3.1.2), it is possible to calculate magnetic field contribution of one corner. Since all three corners are identical and have the same current flow direction, the contribution of one corner is simply multiplied by three to find total contribution of the corners. On the other hand, in addition to magnetic field contributions of rounded corners, contribution of straight parts on the edges should also be calculated. To calculate magnetic field created by the edges, it is required to geometrically analyze the coil shape and derive equations to find edge length and its distance to the center point. In Figure 3.1.3 triangular coil geometry having rounded corners is illustrated once again with geometrical parameters.

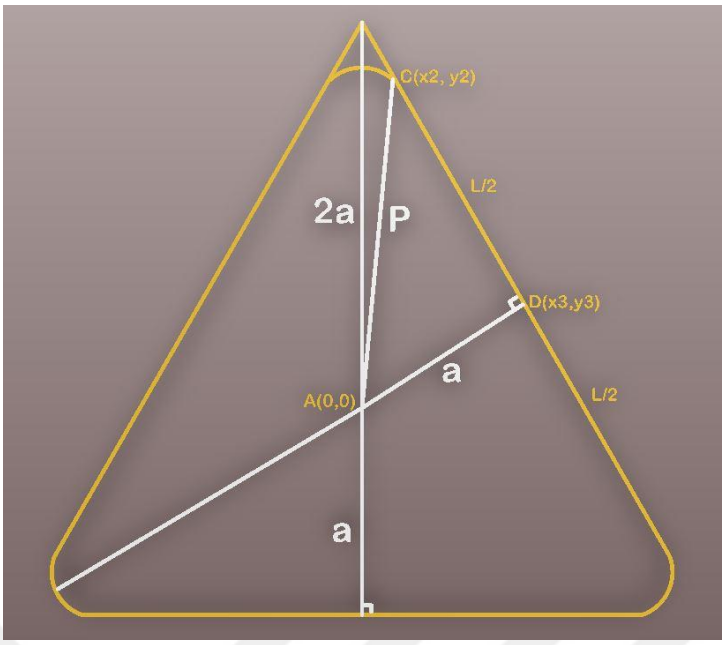

Figure 3.1.2 Triangular coil structure with geometrical parameters.

Different from the previous figures, in Figure 3.1.2, *a* represents the shortest distance between the coil center point A(0, 0) and edges. Similarly, *p* stands for the distance between the coil center (A(0, 0)) and start (or end ($C(x_2, y_2)$)) points of the arcs. Also, *L* is the length of the straight edges, and *v* is half side length in case of there is no rounding. Relations between parameters *a*, *l*, *p*, *v* and corresponding values of the point C on x and y axes, i.e., x_2 and y_2, are given in the following equations.

$$a = \frac{\sqrt{3 * v^2}}{3} \tag{3.1.3}$$

$$P = \sqrt{a^2 + (\frac{L}{2})^2} \tag{3.1.4}$$

$$P = \sqrt{x_2^{\,2} + y_2^{\,2}} \tag{3.1.5}$$

When (3.1.5) is placed in to (3.1.4), *L* is found as following;

$$L = 2 * \sqrt{x_2^{\,2} + y_2^{\,2} - a^2} \tag{3.1.6}$$

As seen in equation (3.1.3), it is sufficient to know side length of the coil to calculate the parameter *a*. Similarly, as seen in equation (3.1.6), one can calculate the parameter *L* if the x and y axes values of the start or end points of the arcs are known together with the coil side length. These observations are important because to easily calculate the magnetic flux density contribution of the edges it is sufficient to find out the parameters *a* and *L*.

3.2 Calculated Magnetic Flux Density Results

After completing derivations, we calculated magnetic flux densities generated by triangular shaped coils with three different sizes that are the same with the sizes of squircle shaped coils reported in chapter 2. As in squircle shaped coils, side lengths of the triangular shaped coils are set to be 7.5 cm, 16.0 cm, and 28.0 cm. In addition, for each coil size, calculations were repeated for different amounts of rounding.

As in squircle coils, here calculations are done for two different triangular coil geometries. In the first geometry, arcs at the corners are parts of the same circle such that center of this circle containing the arcs coincide with the center point of the triangular coil. On the other hand, in the second triangular coil geometry, arcs at the corners are parts of circles such that center points of these circles are distinct and these center points of the circles do not need to be coinciding with the center point of the triangular coil. In both cases, magnetic flux density contributions of the arcs and straight edges were calculated. Arcs and edges of the triangular geometries in both cases are assumed to have same lengths and same distances to the coil center. In other words, arcs and edges of the investigated triangular geometries are symmetric with respect to coil center. Therefore, total magnetic flux density created by the triangular shaped coils can be found by first calculating magnetic flux density contributions of an edge and an arc; and then multiplying these contribution results by three. In all the flux density calculations, to make fair comparison flowing current amplitude on coils is set to be 1 A. Obtained results for the cases are given in the flowing pages.

3.2.1 Case 1: Triangular Geometry with Arcs Containing by a Circle whose Center is Coinciding with the Center Point of the Triangular Geometry

We first made magnetic flux density calculations for the first case in which triangular coil geometry with arcs that are parts of the same circle is investigated. Center of the circle that is assumed to contain rounding corners, i.e., arcs, of the coil is coinciding with the coil center, i.e., centroid of the triangle shaped coil in the first case. Such a specific geometry of a coil allows us to calculate total magnetic flux density created by the coil at its center by using both our proposed and traditional methods. As a result, it is possible to make a fair comparison between the methods and to calculate amount of error

of the results obtained with the derived formula compared to results found by formulas exist in literature.

Calculations were repeated for coils having different side lengths and different amounts of rounding. In Fig. 3.2.1.1 triangular shaped coils with a side length of 8 cm and having different amounts of rounding at the corners are illustrated.

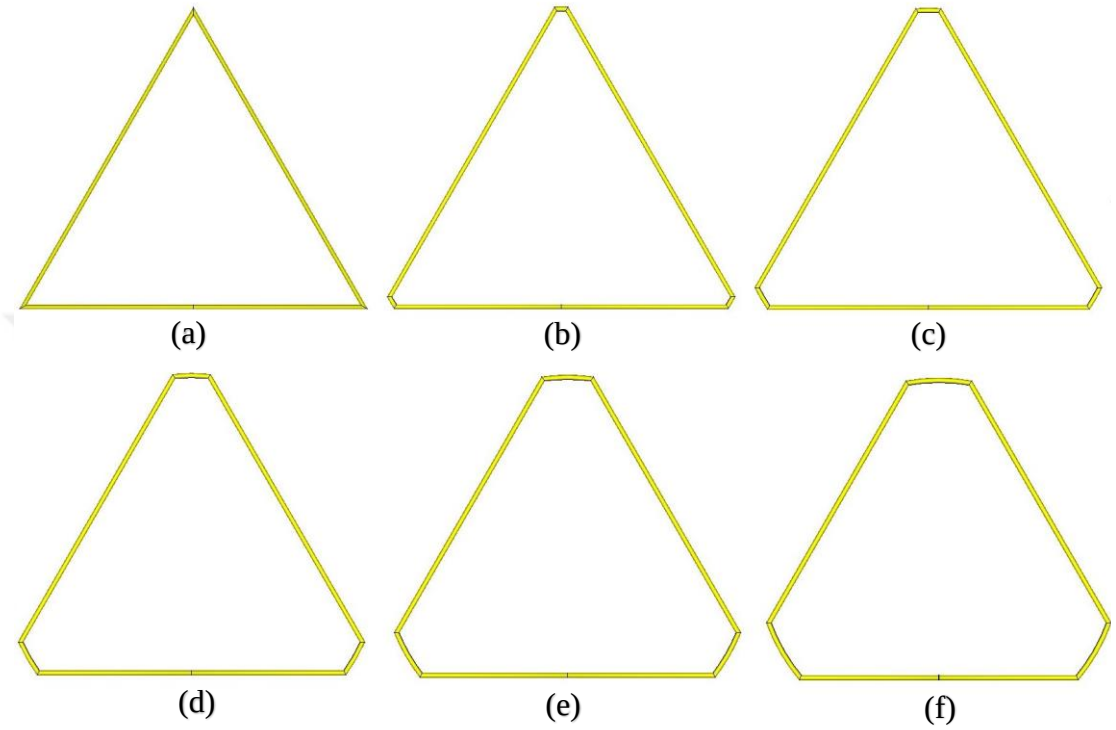

Figure 3.2.1.1 Triangular shaped coils with different amounts of rounding at the corners. Here, side length of the coils is selected to be 16 cm and length of the straight parts (*L* in Fig. 3.1.3) is (a) 16 cm, (b) 15 cm, (c) 14 cm, (d) 13 cm, (e) 12 cm, and (f) 11 cm. In addition, here center of the circle containing the arcs is selected to be coinciding with the coil center, i.e., point A(0,0) in Fig. 3.1.3.

As we did in chapter 2 for the squircle coils, geometrical parameters of triangular shaped coils investigated in case 1 were calculated and they are given in Table 3.2.1.1, Table 3.2.1.2, and Table 3.2.1.3 for coils side length equal to 7.5 cm, 16.0 cm, and 28.0 cm, respectively. In the tables, the first and second parameters named as “Arc Start Point” and “Arc End Point” indicate coordinates of the start and end points (points B(x_1, y_1) and C(x_2, y_2) in Fig. 3.1.2), respectively, of the arc located at the top in the represented triangular coil geometries. On the other hand, the parameters named “Arc Length” and “Edge Length” describe lengths of an arc and an edge, respectively, in unit of cm. Because of symmetry of the triangular coil geometry in case 1, start and end points of the other arcs at the corners can easily be found. In addition, it is important that all the arcs are

assumed to have the same length in the investigated triangular geometry. The fifth parameter in the tables named as “Arc Radius”, corresponds to radius of the circle that contains the arc (distance *r* in Figure 3.1.2). As in squircle coils, the triangular geometry in case 1 is arranged such that center of the circle containing the arcs coincide with the mass center of the triangle geometry. Coordinates of this point are represented in the tables with the sixth parameter named as “Center Coordinates” and they are selected as (0, 0). Finally, the last parameter in the table named “Arc Angle” is the central angle of an arc (θ_1 in equation (3.1.1)).

Arc Start Point (cm, cm)	**Arc End Point (cm, cm)**	**Arc Length (cm)**	**Edge Length (cm)**	**Arc Radius (cm)**	**Center Coordinates (cm, cm)**	**Arc Angle (radian)**
(0, 4.33)	(0, 4.33)	0	3.75	0	(0, 0)	0
(0.25, 3.89)	(-0.25, 3.89)	0.50034	3.25	3.90512	(0, 0)	0.12812
(0.50, 3.46)	(-0.5, 3.46)	1.00343	2.75	3.50000	(0, 0)	0.28669
(0.75, 3.03)	(-0.75, 3.03)	1.51481	2.25	3.12249	(0, 0)	0.48512
(1.00, 2.59)	(-1.00, 2.59)	2.04571	1.75	2.78388	(0, 0)	0.73484

Table 3.2.1.1 Geometrical parameters of triangular shaped coil with a side length equal to 7.5 cm having different amounts of rounding.

Arc Start Point (cm, cm)	**Arc End Point (cm, cm)**	**Arc Length (cm)**	**Edge Length (cm)**	**Arc Radius (cm)**	**Center Coordinates (cm, cm)**	**Arc Angle (radian)**
(0, 9.23)	(0, 9.23)	0	8.0	9.23760	(0, 0)	0
(0.25, 8.80)	(-0.25, 8.80)	0.50006	7.5	8.80814	(0, 0)	0.05677
(0.50, 8.37)	(-0.50, 8.37)	1.00059	7.0	8.38649	(0, 0)	0.11931
(0.75, 7.93)	(-0.75, 7.93)	1.50222	6.5	7.97391	(0, 0)	0.18839
(1.00, 7.50)	(-1.00, 7.50)	2.00586	6.0	7.57187	(0, 0)	0.26490
(1.25, 7.07)	(-1.25, 7.07)	2.51279	5.5	7.18215	(0, 0)	0.34986

Table 3.2.1.2 Geometrical parameters of triangular shaped coil with a side length equal to 16.0 cm having different amounts of rounding.

Arc Start Point (cm, cm)	Arc End Point (cm, cm)	Arc Length (cm)	Edge Length (cm)	Arc Radius (cm)	Center Coordinates (cm, cm)	Arc Angle (radian)
(0, 16.16)	(0, 16.16)	0	14.0	16.1658	0	0
(0.25, 15.73)	(-0.25, 15.73)	0.50002	13.5	15.7347	0	0.031778
(0.50, 15.29)	(-0.50, 15.29)	1.00017	13.0	15.3079	0	0.065337
(0.75, 14.86)	(-0.75, 14.86)	1.50063	12.5	14.8856	0	0.100810
(1.00, 14.43)	(-1.00, 14.43)	2.00159	12.0	14.4683	0	0.138342
(1.25, 14.00)	(-1.25, 14.00)	2.50330	11.5	14.0564	0	0.178089

Table 3.2.1.3 Geometrical parameters of triangular shaped coil with a side length equal to 28.0 cm having different amounts of rounding.

When the tables are examined, it is seen that each coil having different side lengths starts with a complete equilateral triangle shape such that the arc lengths are zero, and continue with increased arc length which indicates enhanced rounding at the corners. Increasing arc length allows us to see rounding affect on the created magnetic flux density at the center of the coil.

Calculated magnetic flux densities created by the coils at the center are given for different amounts of rounding in Table 3.2.1.4, Table 3.2.1.5, and Table 3.2.1.6 with side lengths equal to 7.5 cm, 16.0 cm, and 28.0 cm, respectively.

Arc Start Point (cm, cm)	Magnetic Flux Density Calculated by Proposed Method (Wb/cm^2)	Magnetic Flux Density Calculated by Traditional Method (Wb/cm^2)	Error Between Proposed and Traditional Methods (%)
(0, 4.33)	2.4000000000E-05	2.4000000000E-05	0.00000000
(0.25, 3.89)	2.4047983293E-05	2.4047983316E-05	0.00000009
(0.50, 3.46)	2.4231739763E-05	2.4231739905E-05	0.00000059
(0.75, 3.03)	2.4630163195E-05	2.4630163705E-05	0.00000207
(1.00, 2.59)	2.5339697668E-05	2.5339699130E-05	0.00000577

Table 3.2.1.4 Calculated magnetic flux density of triangular shaped coil with a side length equal to 7.5 cm having different amounts of rounding.

Arc Start Point (cm, cm)	Magnetic Flux Density Calculated by Proposed Method (Wb/cm^2)	Magnetic Flux Density Calculated by Traditional Method (Wb/cm^2)	Error Between Proposed and Traditional Methods (%)
(0, 9.23)	1.1250000000E-05	1.1250000000E-05	0.00000000
(0.25, 8.80)	1.1254482202E-05	1.1254482202E-05	0.00000001
(0.50, 8.37)	1.1269540530E-05	1.1269540535E-05	0.00000004
(0.75, 7.93)	1.1297991294E-05	1.1297991305E-05	0.00000010
(1.00, 7.50)	1.1343231413E-05	1.1343231439E-05	0.00000023
(1.25, 7.07)	1.1409265003E-05	1.1409265054E-05	0.00000044

Table 3.2.1.5 Calculated magnetic flux density of triangular shaped coil with a side length equal to 16.0 cm having different amounts of rounding.

Arc Start Point (cm, cm)	Magnetic Flux Density Calculated by Proposed Method (Wb/cm^2)	Magnetic Flux Density Calculated by Traditional Method (Wb/cm^2)	Error Between Proposed and Traditional Methods (%)
(0, 16.16)	6.4285714286E-06	6.4285714286E-06	0.00000000
(0.25, 15.73)	6.4293778980E-06	6.4293778981E-06	0.00000000
(0.50, 15.29)	6.4319577845E-06	6.4319577849E-06	0.00000001
(0.75, 14.86)	6.4365743758E-06	6.4365743767E-06	0.00000002
(1.00, 14.43)	6.4435231494E-06	6.4435231514E-06	0.00000003
(1.25, 14.00)	6.4531341660E-06	6.4531341694E-06	0.00000005

Table 3.2.1.6 Calculated magnetic flux density of triangular shaped coil with a side length equal to 28.0 cm having different amounts of rounding.

In the tables, arc start points are given to understand amount of rounding for different sized coils. Besides that, overall magnetic flux densities calculated by the proposed and traditional methods are given in the tables. Since center of the circle containing the arcs are selected to be coinciding with the mass center of the triangle shape coil, in case 1 it is possible to make fair comparison between the results. Therefore, error is calculated between the results found by following the two methods and given in the tables in percentage. As seen, the maximum error is calculated to be far below 0.001 %. Such a very low error rate proves the correctness of derived formulation in this study.

3.2.2 Case 2: Triangular Geometry with Arcs Containing by Different Circles whose Centers are not Coinciding with the Center Point of the Triangular Geometry

After proving correctness of the proposed formula for the triangular coil geometry in case 1, in case 2 magnetic flux density created by a triangular coil with geometry different than the coil geometry in case 1 at its center is calculated. Here, the coil geometry is different such that arcs at the corners occurred as a result of rounding are contained by different circles whose centers are not coinciding with the center point of the triangular geometry. However, as in the previous case, in the second case arcs at the corners are assumed to be identical and symmetric with respect to coil center.

As in previous case, magnetic flux density calculations were repeated for different sized coils. For each size, rounding of the corners is changed. However, for fair comparison, total length of coils is kept constant. More clearly, in this case, the total length of each size of coil is first determined by using their triangular shaped forms with sharp corners. Then different amounts of rounding are applied by keeping total length fixed. By this way, it is possible to see effects of rounding to magnetic flux density created at the coil center. In Figure 3.2.2.1, triangular shaped coils with different amounts of rounding at the corners are shown. Coils represented in the figure have constant total length equal to 48 cm and straight edges with length equal to 16 cm, 15 cm, 14 cm, 13 cm, 12 cm, and 11 cm in subfigures (a), (b), (c), (d), (e), and (f), respectively.

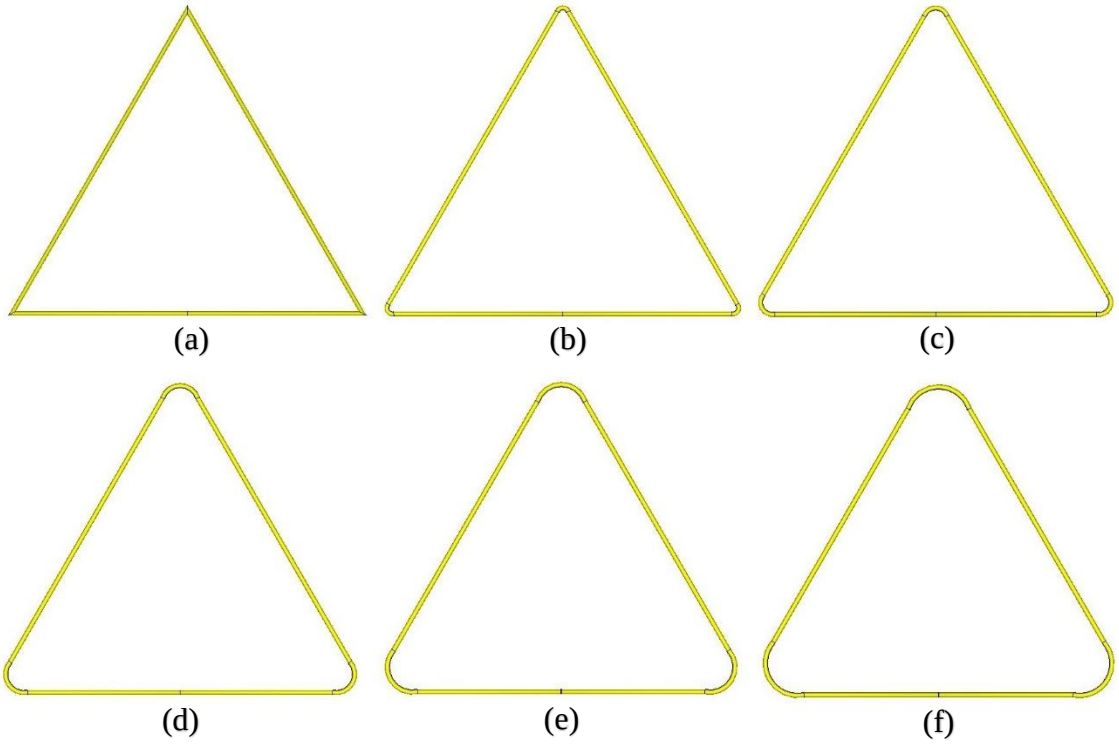

Figure 3.2.2.1 Triangular shaped coils with different amounts of rounding at the corners. Here, total length of the coils is selected to be constant 48 cm and length of the straight parts is (a) 16 cm, (b) 15 cm, (c) 14 cm, (d) 13 cm, (e) 12 cm, (f) 11 cm. In addition, here centers of the circles containing the arcs are selected to be not coinciding with the coil center.

Before calculating magnetic flux densities created by the coils at their center points, it is required to calculate some geometrical parameters, i.e., start and end points of an arc, arc length, radius and center point coordinates of circle containing the arc. Among them, radius and center point coordinates of circle containing the arc are found by iteratively solving the equations (2.3.2.6), (2.3.2.7), and (2.3.2.8) those exist in chapter 2. Geometrical parameters of triangular shaped coils having different corner roundings investigated in case 2 are given in Table 3.2.2.1, Table 3.2.2.2, and Table 3.2.2.3 for coil total side lengths equal to 22.5 cm, 48.0 cm, and 84.0 cm, respectively.

Arc Start Point (cm, cm)	**Arc End Point (cm, cm)**	**Arc Length (cm)**	**Found Arc Length (cm)**	**Found Arc Radius r (cm)**	**Found Center Coordinates (cm, cm)**
(0, 4.33)	(0, 4.33)	0	0	0	0
(0.25, 3.89)	(-0.25, 3.89)	1	0.99996650	0.26378	(0, 3.81297224)
(0.50, 3.46)	(-0.50, 3.46)	2	2.00003034	0.52757	(0, 3.29578612)
(0.75, 3.03)	(-0.75, 3.03)	3	2.99999685	0.79135	(0, 2.77863134)
(1.00, 2.59)	(-1.00, 2.59)	4	3.99996336	1.05513	(0, 2.26147657)

Table 3.2.2.1 Geometrical parameters of triangular shaped coil with a total length equal to 22.5 cm having different amounts of rounding.

Arc Start Point (cm, cm)	**Arc End Point (cm, cm)**	**Arc Length (cm)**	**Found Arc Length (cm)**	**Found Arc Radius r (cm)**	**Found Center Coordinates (cm, cm)**
(0, 9.23)	(0, 9.23)	0	0	0	0
(0.25, 8.80)	(-0.25, 8.80)	1	0.99996650	0.26378	(0, 8.72044953)
(0.50, 8.37)	(-0.50, 8.37)	2	2.00003034	0.52757	(0, 8.20326341)
(0.75, 7.93)	(-0.75, 7.93)	3	2.99999685	0.79135	(0, 7.68610863)
(1.00, 7.50)	(-1.00, 7.50)	4	3.99996336	1.05513	(0, 7.16895386)
(1.25, 7.07)	(-1.25, 7.07)	5	5.00002720	1.31892	(0, 6.65176773)

Table 3.2.2.2 Geometrical parameters of triangular shaped coil with a total length equal to 48.0 cm having different amounts of rounding.

Arc Start Point (cm, cm)	**Arc End Point (cm, cm)**	**Arc Length (cm)**	**Found Arc Length (cm)**	**Found Arc Radius r (cm)**	**Found Center Coordinates (cm, cm)**
(0, 16.16)	(0, 16.16)	0	0	0	0
(0.25, 15.73)	(-0.25, 15.73)	1	0.99996650	0.26378	(0, 15.6486527)
(0.50, 15.29)	(-0.50, 15.29)	2	2.00003034	0.52757	(0, 15.1314666)
(0.75, 14.86)	(-0.75, 14.86)	3	2.99999685	0.79135	(0, 14.6143118)
(1.00, 14.43)	(-1.00, 14.43)	4	3.99996336	1.05513	(0, 14.0971570)
(1.25, 14.0)	(-1.25, 14.0)	5	5.00002720	1.31892	(0, 13.5799709)

Table 3.2.2.3 Geometrical parameters of triangular shaped coil with a total length equal to 84.0 cm having different amounts of rounding.

In the tables, as in the previous case, geometrical parameters of the arcs and circles containing the arcs are given. Parameter in the third column named as “Arc Length” is length of the arc that is known due to fixed total length. On the other hand, the other parameter named as “Found Arc Length” is the arc length calculated by using equation (2.3.2.6), where *S* represents this parameter. Similarly, parameters “Found r” and “Found Center Coordinates” are calculated by using equations (2.3.2.7) and (2.3.2.8). As seen in the tables, found arc lengths are very close to real arc lengths. In addition, in the tables it is seen that center point of the circle containing the arcs do not coincide with the center of the coil. Therefore, in the second case for the investigated triangular coil geometry it is not possible to use traditional formulas to calculate created magnetic flux density. However, we calculated magnetic flux densities at the center of the coils having different roundings by using our derived formulas. Magnetic flux densities at the center of

triangular shaped coils in case 2 are given in Table 3.2.2.4, Table 3.2.2.5, and Table 3.2.2.6 for coil total lengths equal to 22.5 cm, 48.0 cm, and 84.0 cm, respectively.

Arc start Point (cm, cm)	Magnetic Flux Density Created by Edges (Wb/cm^2)	Magnetic Flux Density Created by Arcs Calculated by Using Proposed Formula (Wb/cm^2)	Overall Magnetic Flux Density Created by Coil (Wb/cm^2)
(0, 4.33)	2.40000E-05	0.00	2.40000E-05
(0.25, 3.89)	2.30637E-05	9.54196E-07	2.40179E-05
(0.50, 3.46)	2.17744E-05	2.30773E-06	2.40821E-05
(0.75, 3.03)	1.99692E-05	4.24427E-06	2.42135E-05
(1.00, 2.59)	1.74208E-05	7.02195E-06	2.44427E-05

Table 3.2.2.4 Calculated magnetic flux density and its contributors in triangular shaped coils with a total length equal to 22.5 cm and having different amounts of rounding.

Arc start Point (cm, cm)	Magnetic Flux Density Created by Edges (Wb/cm2)	Magnetic Flux Density Created by Arcs Calculated by Using Proposed Formula (Wb/cm2)	Overall Magnetic Flux Density Created by Coil (Wb/cm2)
(0, 9.23)	1.12500E-05	0.00	1.12500E-05
(0.25, 8.80)	1.10611E-05	1.90604E-07	1.12517E-05
(0.50, 8.37)	1.08427E-05	4.14567E-07	1.12573E-05
(0.75, 7.93)	1.05892E-05	6.78313E-07	1.12675E-05
(1.00, 7.50)	1.02937E-05	9.89576E-07	1.12832E-05
(1.25, 7.07)	9.94786E-06	1.35762E-06	1.13055E-05

Table 3.2.2.5 Calculated magnetic flux density and its contributors in triangular shaped coils with a total length equal to 48.0 cm and having different amounts of rounding.

Arc start Point (cm, cm)	Magnetic Flux Density Created by Edges (Wb/cm2)	Magnetic Flux Density Created by Arcs Calculated by Using Proposed Formula (Wb/cm2)	Overall Magnetic Flux Density Created by Coil (Wb/cm2)
(0, 16.16)	6.42857E-06	0.00	6.42857E-06
(0.25, 15.73)	6.36879E-06	6.00945E-08	6.42888E-06
(0.50, 15.29)	6.30391E-06	1.25954E-07	6.42987E-06
(0.75, 14.86)	6.23340E-06	1.98184E-07	6.43159E-06
(1.00, 14.43)	6.15667E-06	2.77458E-07	6.43413E-06
(1.25, 14.00)	6.07305E-06	3.64527E-07	6.43757E-06

Table 3.2.2.6 Calculated magnetic flux density and its contributors in triangular shaped coils with a total length equal to 84.0 cm and having different amounts of rounding.

In the tables it is seen that magnetic flux density contributions created by the edges decrease as the rounding at the corners increases. This is expected because as the rounding decreases straight edges become shorter. On the other hand, magnetic flux density

contributions created by the arcs at the corners increase as the rounding increases. This is also an expected result because as the rounding increases length of arcs at the corners increase, too. Because of enhanced contribution of the arcs that eliminates decrease in contribution of the straight edges, in the table total magnetic flux density created at the center of the coils increase. As an example, total magnetic flux density variation with respect to start points of an arc on x-axis for the triangular shaped coils in case 2 having a 48 cm circumferential length is shown in Figure 3.2.2.2.

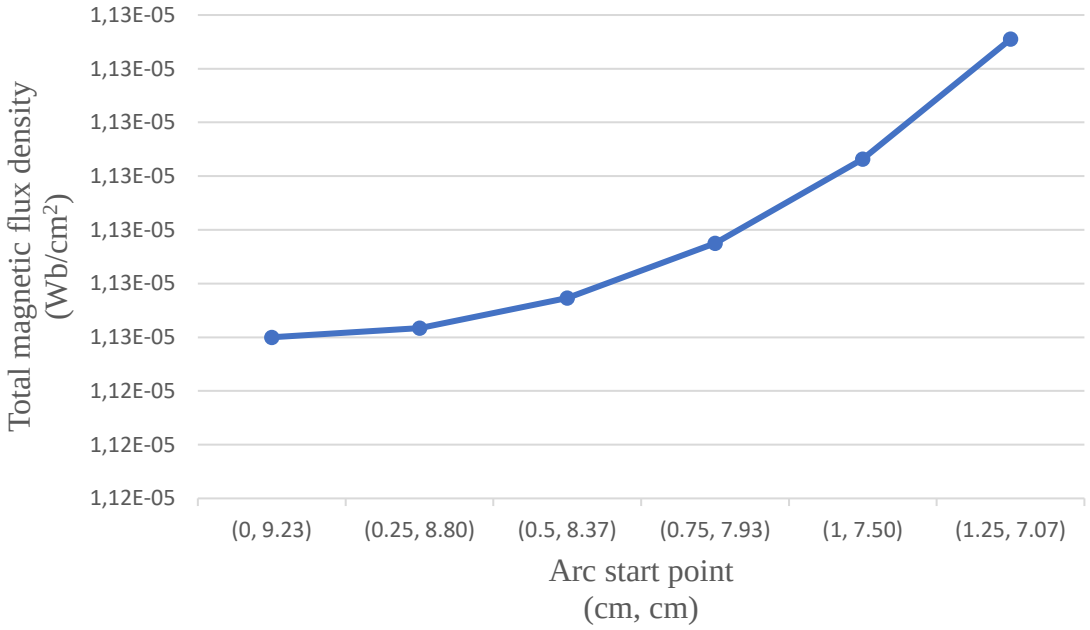

Figure 3.2.2.2 Change of total magnetic flux density calculated at the center of squircle shaped coils having a 48 cm circumferential length with respect to start points on x-axis.

In the figure, while the point of (0, 9.23) represents zero-rounding, the point (1.25, 7.07) represents maximum amount of rounding. As expected, total magnetic flux density increases with the rounding. However, this increase is different from the increase observed in chapter 2 for the squircle shaped coils (see Figure 2.3.2.3). Because there is no formulation in literature to calculate results of the fixed total length case, obtained results cannot be verified by comparing with any other result. However, the calculated results were verified by the simulations that are presented in the next chapter.

Chapter 4

Simulations

In the previous chapters, we analytically derived formulas of magnetic flux density and some geometrical parameters including arc length, center point coordinates of arc, and so on. We achieved to calculate magnetic field and flux density contributions of any rounded corner at the center of a coil. To prove the correctness of the derived formulas, magnetic flux densities at the center of coils with two different geometries that are square and triangular shapes with rounded corners were calculated. In addition, for each geometry two different cases were investigated. In the first case, roundings in the corners are set to be parts of the same circle and center point of this circle that contains the arcs coincides with the center point (mass center point) of the coils. In the first cases of the squircle and triangular shaped coils, magnetic flux densities created by the coils at the center point were calculated by using the proposed formulas and the formulas exist in literature. The results were compared and they are given in the previous chapters. It is seen that the maximum error between the results calculated with the proposed and traditional formulas is lower than 0.3%. One of the reasons to obtain difference between the calculated results is a limited accuracy of the numerical calculations.

Next, the calculations were repeated for the second case. In case 2, to analyze how production difficulties affect magnetic field created by a coil, magnetic flux density created by a coil at its center was calculated for various amounts of rounding at the corners by keeping total length of the coil constant. For different roundings at the corners to keep total coil length constant, arc shapes turn into being protruding. It means, in the second case geometries of the square and triangular shaped coils having rounded corners, arcs are parts of circles located at different positions. In addition to these geometries, centers of coils containing the arcs are not coinciding with the coil center. Therefore, for the coil geometries examined in the second cases, magnetic flux densities were calculated by using only our derived formulas. However, to verify the calculated results, we conducted

three-dimensional (3D) electromagnetic (EM) simulations. In the simulations, magnetic flux densities created by the coils were found. Simulations are explained below in details together with the found results. In addition, comparisons are made between the results analytically calculated and calculated in simulations.

4.1 Finite Element Modeling

Solving complex engineering problems in nature are quite complex. Especially, if geometries of the materials and mediums are complex and their behaviors or responses are nonlinear then it might not be possible to solve mathematical equations that model responses of the materials in the medium. To solve mathematical equations in complex geometries one effective method is to discretize the domain, in other words to divide the volume (or surface, or line, etc.) into subdomains and solve the equations in these subdomains. These discrete subdomains are called finite elements and they are chosen to be simple, small, and interconnected to yield correct results. Because of discretization finite element modeling enables approximated results. Accuracy of the results depends on quality of the modeling but with finite element modeling a complex problem is simplified. In short, in finite element modeling the idea is to enable a relatively large model to be solved more easily by dividing it into easily solvable, interconnected pieces with a plurality of nodes.

4.1.1 Simulation Software

Since finite element method simplifies complex problems, it is widely used in computer-based simulation tools. In this study, the simulations were done for different shapes and amounts of rounding by using one of these tools, which is called CST STUDIO. It is preferred due to the advantages of having student version, being a strong tool, and being well documented. CST STUDIO includes different solvers. Depending on problem type the most appropriate solver is used to obtain the best solutions. In our cases, we performed our simulations in M-Static solver with low-frequency problem type set.

4.1.2 Coil Drawings

In the simulations, coil structures are constructed initially with help of the tools provided by the software. The coil geometrical parameters such as arc length, radius and center coordinates of circles that contain the arcs, etc. are set in the simulations to be same with the parameters analytically calculated. Also, in the simulations material of the coil is selected as copper and the wire radius is set to be 0.01 cm. As an example, constructed triangular and squircle coils in case 1 with side lengths equal to 16 cm are shown in figure 4.1.2.1. In the squircle coil, length of straight edges and length of arcs are 10 cm and 7.29 cm, respectively.

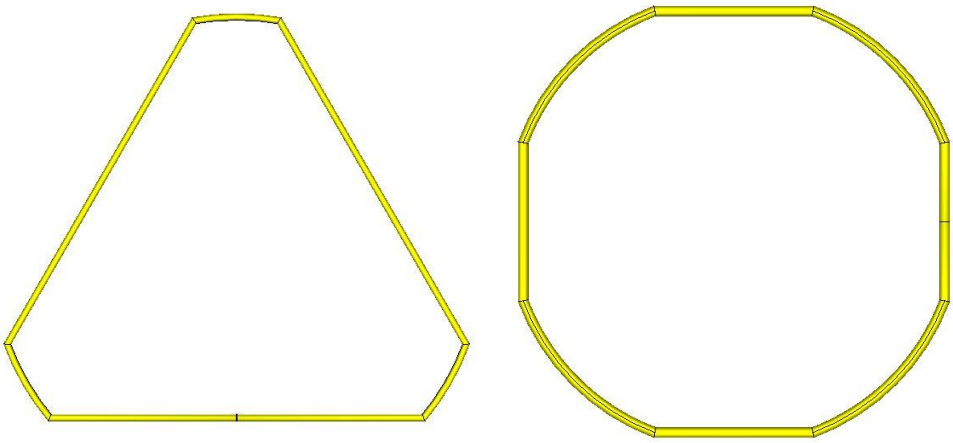

(a) (b)

Figure 4.1.2.1 Exemplary coil structures constructed in simulation software. (a) Triangular coil having 16 cm side length, (b) Squircle coil having 16 cm side length.

4.1.3 Current Port

For a coil to produce magnetic field, there should be an alternating (a.c.) current flowing on it. One way to yield an alternating current flow on a coil in CST is to use a current port. To this end, we removed a very small piece of wire from the coils and placed a current port into this slit such that two ends of the port are in contact with copper wire from its opposite sides. A current port placed between two end points of a squircle coil exists in one of our simulated structures is shown in figure 4.1.3.1. In all the simulations, current value was set to be 1 A and operating frequency was adjusted to be 20 KHz.

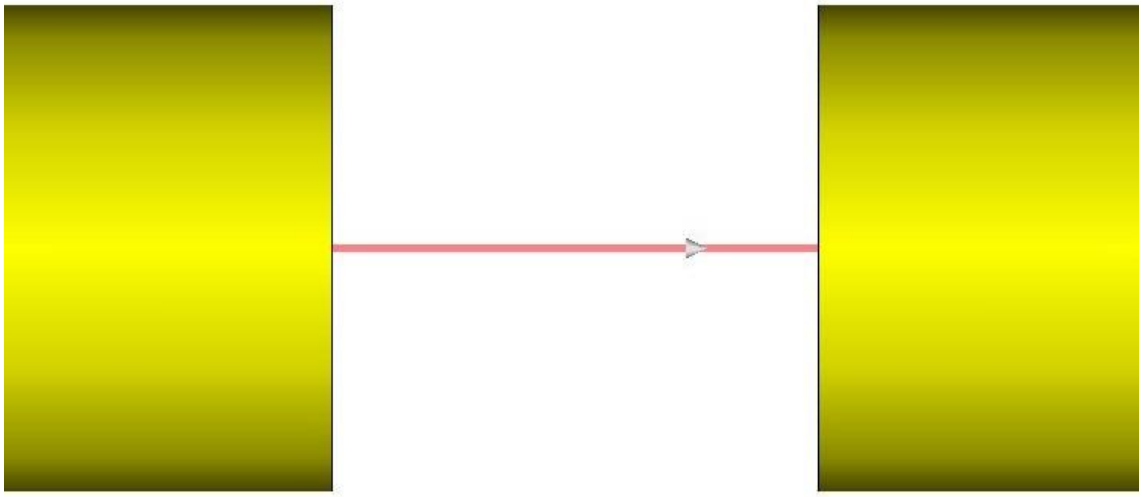

Figure 4.1.3.1 Part of a simulated squircle coil together with a current port placed between two end points of the coil.

4.1.4 Meshing

A grid-like structure formed by nodes is called a mesh. In a meshed structure material information determines how the structure will behave under certain loading conditions. In our simulations, tetrahedral meshes are used for meshing squircle and triangular shaped coils because of their curved architectures. As an exemplary, a squircle shaped coil meshed with tetrahedral meshes is shown in figure 4.1.4.1.

Magnetic flux densities were calculated with different number of meshes. It is seen that as the meshing accuracy increases calculated magnetic flux densities change. However, after some point results do no change considerably, i.e., results converge to values. Our calculated magnetic flux densities in the simulations are converged results and they are almost the same with the results found analytically.

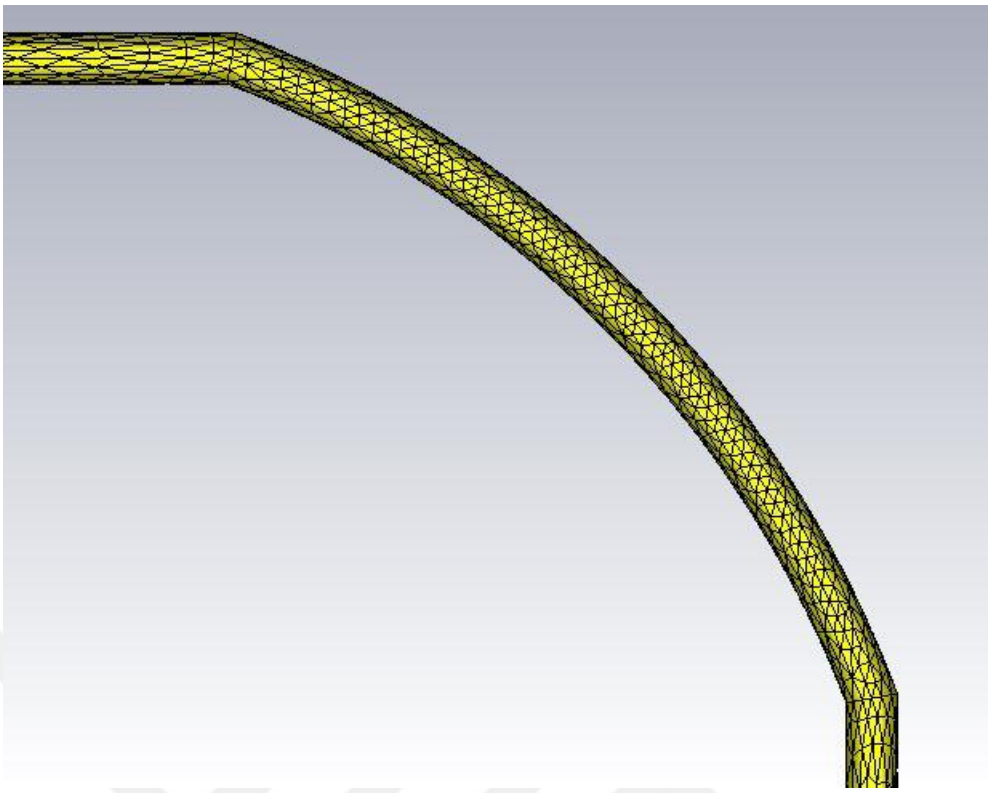

Figure 4.1.4.1 Part of a squircle coil meshed with tetrahedral meshes in our simulations.

4.1.5 Background Material

The materials being simulated can be in different mediums such as air, water, and so on. Because each medium may have different electromagnetic and physical properties and parameters such as different electrical permittivity, magnetic permeability, material density, etc., system responses and so obtained simulation results are found to be different accordingly. In our analysis, we assumed that our coils are in free-space. Therefore, in the simulations, we select free-space as the background material.

4.1.6 Boundary Selection

Another setting that needs to be adjusted in electromagnetic simulations is boundary condition. Depending on simulating structure and the medium that the structure is placed inside boundary selection should be carefully made. One of the boundaries exist in CST is open boundary. Open boundary condition models a system to be placed in an infinite free-space. Therefore, in open boundary condition cases electromagnetic reflection from the boundaries are minimized. Since in our analysis we assumed that coils are placed in a free-space, which is necessary to correctly find magnetic flux density

created only by the coil itself, in the simulations we used open boundary conditions in all directions.

4.2 Squircle Coil Simulations

We first conducted simulations for the squircle shaped coils. The coils in the simulations were constructed to have the same geometries with the coils investigated in chapter 2. Therefore, in the simulations we used the geometrical parameters calculated for squircle shaped coils in chapter 2. As we did in theoretical analysis, simulations were repeated for two different cases. In the first case, arcs at the corners of squircle coil geometry are assumed to be parts of a circle whose center is coinciding with the center of the coil. In the second case, however, arcs at the corners are assumed to be parts of circles positioned at different locations and center points of these circles that contain the arcs are different than the center point of the circle.

In Figure 4.2.1, magnetic flux density distribution calculated in our simulations for a squircle shaped coil is illustrated. In the figure, coil is represented with yellow and magnetic flux densities are pointed out with blue dots such that in the regions where blue dots are dense magnetic flux densities are high.

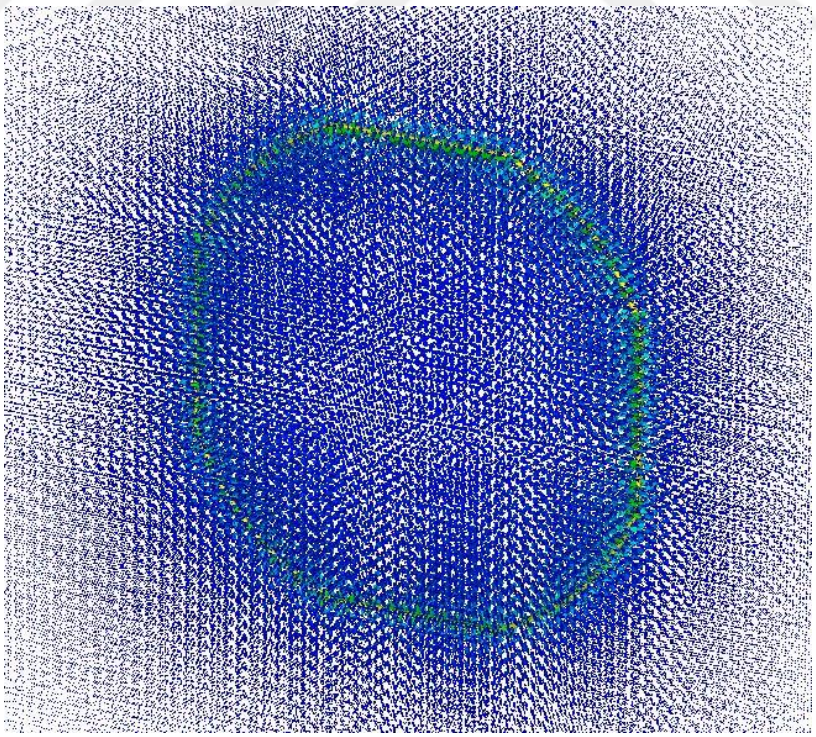

Figure 4.2.1 Magnetic field density distribution over the coil in simulation software.

4.2.1 Case 1 Results

Simulations were done initially for squircle coils in case 1. As it is explained in chapter 2, magnetic flux densities created by the coils at their centers were calculated by using the derived formulas and the formulas exist in literature. On the other hand, we also simulated the coils that were analytically investigated before in chapter 2. By this way, we aimed to verify correctness of our simulations. Magnetic flux densities of squircle shaped coils at their centers analytically calculated by using our proposed method and the traditional method that exists in literature together with the flux densities calculated in the simulations are given in Table 4.2.1.1, Table 4.2.1.2, and Table 4.2.1.3 for various rounding amounts and coil side lengths equal to 7.5 cm, 16.0 cm, and 28.0 cm, respectively. In the tables, error between the results analytically found by using the proposed method and calculated in simulations is given, too.

Arc Start Point (cm, cm)	**Magnetic Flux Density Calculated by Proposed Method (Wb/cm^2)**	**Magnetic Flux Density Calculated by Traditional Method (Wb/cm^2)**	**Magnetic Flux Density Calculated in Simulations (Wb/cm^2)**	**Error between Proposed Method Results and Simulation Results (%)**
(3.74, 3.75)	1.5087E-05	1.5085E-05	1.4985E-05	0.68
(2.50, 3.75)	1.5337E-05	1.5337E-05	1.5310E-05	0.18
(1.25, 3.75)	1.6111E-05	1.6130E-05	1.6097E-05	0.09
(0, 3.75)	1.6710E-05	1.6755E-05	1.6719E-05	0.05

Table 4.2.1.1 Calculated magnetic flux densities of squircle shaped coils in case 1 with a side length equal to 7.5 cm having different amounts of rounding.

Arc Start Point (cm, cm)	**Magnetic Flux Density Calculated by Proposed Method (Wb/cm^2)**	**Magnetic Flux Density Calculated by Traditional Method (Wb/cm^2)**	**Magnetic Flux Density Calculated in Simulations (Wb/cm^2)**	**Error between Proposed Method Results and Simulation Results (%)**
(7.99, 8.00)	7.0738E-06	7.0711E-06	7.0416E-06	0.46
(7.00, 8.00)	7.0910E-06	7.0860E-06	7.0683E-06	0.32
(5.00, 8.00)	7.2253E-06	7.2232E-06	7.2023E-06	0.32
(3.00, 8.00)	7.5091E-06	7.5059E-06	7.4988E-06	0.14
(0, 8.00)	7.8414E-06	7.8540E-06	7.8653E-06	0.30

Table 4.2.1.2 Calculated magnetic flux densities of squircle shaped coils in case 1 with a side length equal to 16.0 cm having different amounts of rounding.

Arc Start Point (cm, cm)	Magnetic Flux Density Calculated by Proposed Method (Wb/cm^2)	Magnetic Flux Density Calculated by Traditional Method (Wb/cm^2)	Magnetic Flux Density Calculated in Simulations (Wb/cm^2)	Error between Proposed Method Results and Simulation Results (%)
(13.99, 14.00)	4.0412E-06	4.0406E-06	4.0198E-06	0.53
(11.00, 14.00)	4.0674E-06	4.0670E-06	4.0460E-06	0.53
(8.00, 14.00)	4.1573E-06	4.1561E-06	4.1385E-06	0.45
(5.00, 14.00)	4.3032E-06	4.3025E-06	4.2909E-06	0.29
(0.00, 14.00)	4.4886E-06	4.4880E-06	4.4672E-06	0.48

Table 4.2.1.3 Calculated magnetic flux densities of squircle shaped coils in case 1 with a side length equal to 28.0 cm having different amounts of rounding.

When the results are examined, it is seen that magnetic flux densities calculated in simulations are very close to those calculated by using the traditional method. This demonstrates that simulations were done correctly. In addition, in the tables, it is also seen that magnetic flux densities found in the simulations are close to magnetic flux densities calculated by using our proposed method such that error between the results are found to be less than 1%. This proves correctness of the proposed formulation.

4.2.2 Case 2 Results

After case 1, we repeated our squircle coil simulations for case 2. In case 2, squircle coils have geometries such that arcs at the corners are parts of circles positioned at different locations and center points of these circles are different than the center point of the coil. We obtained simulations for the coils analytically investigated. To this end, we constructed squircle shaped coils for case 2 with geometrical parameters calculated before in chapter 2. Simulations were repeated for coils having constant total lengths but with different amounts of rounding. Because of the unique geometry of coils in case 2, it is not possible to calculate magnetic field contribution of the arcs by using conventional methods for these coils. Therefore, simulation results are compared only with the results found with the proposed formulas. Magnetic flux densities of squircle shaped coils at their centers analytically calculated by using our proposed method and calculated in the

simulations are given in Table 4.2.2.1, Table 4.2.2.2, and Table 4.2.2.3 for various rounding amounts and coil side lengths equal to 7.5 cm, 16.0 cm, and 28.0 cm, respectively. As in case 1, error between the results is given, too, in the table.

Arc Start Point (cm, cm)	**Magnetic Flux Density Calculated by Proposed Method (Wb/cm^2)**	**Magnetic Flux Density Calculated in Simulations (Wb/cm^2)**	**Error between Proposed Method Results and Simulation Results (%)**
(3.74, 3.75)	1.5085E-05	1.5033E-05	0.35
(2.50, 3.75)	1.5014E-05	1.4947E-05	0.45
(1.25, 3.75)	1.4718E-05	1.4669E-05	0.34
(0, 3.75)	1.4104E-05	1.4068E-05	0.26

Table 4.2.2.1 Calculated magnetic flux densities of squircle shaped coils in case 2 with a side length equal to 7.5 cm having different amounts of rounding.

Arc Start Point (cm, cm)	**Magnetic Flux Density Calculated by Proposed Method (Wb/cm^2)**	**Magnetic Flux Density Calculated in Simulations (Wb/cm^2)**	**Error between Proposed Method Results and Simulation Results (%)**
(7.99, 8.00)	7.0711E-06	7.0438E-06	0.39
(7.00, 8.00)	7.0671E-06	7.0275E-06	0.56
(5.00, 8.00)	7.0272E-06	7.0172E-06	0.14
(3.00, 8.00)	6.9241E-06	6.8858E-06	0.56
(0, 8.00)	6.6112E-06	6.5716E-06	0.60

Table 4.2.2.2 Calculated magnetic flux densities of squircle shaped coils in case 2 with a side length equal to 16.0 cm having different amounts of rounding.

Arc Start Point (cm, cm)	**Magnetic Flux Density Calculated by Proposed Method (Wb/cm^2)**	**Magnetic Flux Density Calculated in Simulations (Wb/cm^2)**	**Error between Proposed Method Results and Simulation Results (%)**
(13.99, 14.00)	4.0406E-06	4.0282E-06	0.31
(11.00, 14.00)	4.0335E-06	4.0019E-06	0.79
(8.00, 14.00)	4.0065E-06	4.0002E-06	0.16
(5.00, 14.00)	3.9507E-06	3.9355E-06	0.38
(0, 14.00)	3.7779E-06	3.7593E-06	0.49

Table 4.2.2.3 Calculated magnetic flux densities of squircle shaped coils in case 2 with a side length equal to 28.0 cm having different amounts of rounding.

When the results are examined, it is seen that simulation results are very close to the results calculated by our proposed method. And similar to case 1, the amount of error in terms of percentage is lower than 1%. This proves correctness of the proposed formulation.

4.3 Triangular Coil Simulations

After completing to derive formulas, it was told that the proposed formula is applicable to any shape of coil that has rounded corners. To demonstrate that, in chapter 3, triangular shaped coils with 3 different sizes that are among the sizes of the coils commonly used in industry are investigated. Magnetic flux densities created by the triangular shaped coils at their centers were calculated by using the derived formulas and the traditional formulas exist in literature. It is seen that the differences between the calculated densities are negligible and it is due to limited accuracies in our calculations. As a result, correctness of the derived formulas to calculate magnetic flux density in a triangular shaped coil having rounded corners was verified. On the other hand, in this section, results of the proposed method are also supported with simulations. Here, as we did for squircle shaped coils, we obtained simulations of triangular shaped coils having rounded corners for two different geometries. In case 1, triangular shaped coils with arcs that are parts of same circle is investigated. Center point of the imaginary circle containing the arcs coincides with the mass center of the triangle shaped coil in this geometry. In case 2, on the other hand, arcs at the corners are assumed to be parts of circles positioned at different locations and center points of these circles do not coincide with the mass center of the triangle shape. Magnetic flux densities were calculated with simulations for both cases. In figure 4.3.1 magnetic flux density distribution over a triangular shaped coil calculated in our simulations is shown. In the figure, as in figure 4.2.1 magnetic flux densities are represented with blue dots.

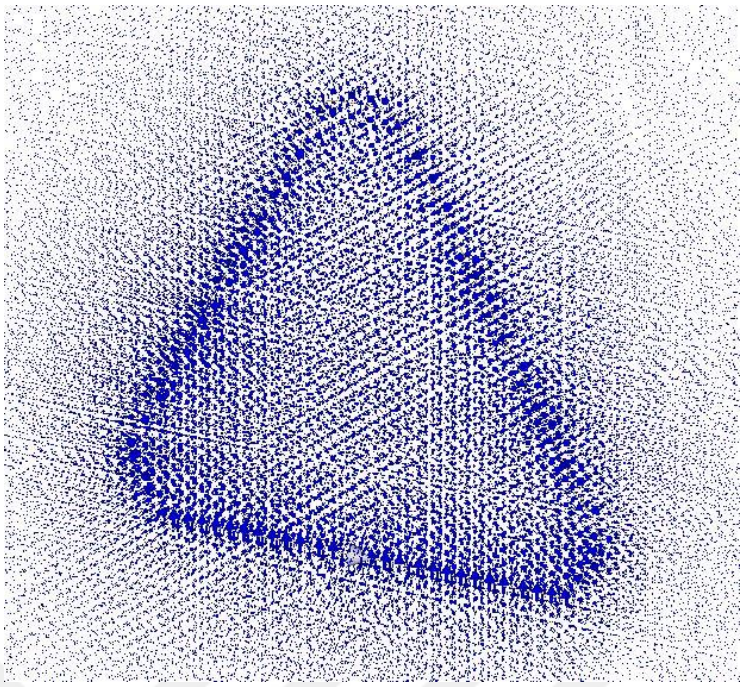

Figure 4.3.1 Magnetic flux density distribution from perspective view over a triangular shaped coil calculated in simulations.

4.3.1 Case 1 Results

We first obtained simulations for triangular shaped coils in case 1. As it is explained in chapter 3, magnetic flux density at the center point of a triangular shaped coil in case 1 is calculated by using our derived formulas and traditional formulas exist in literature. As we did for the squircle shaped coils, we started our triangular shaped coil simulations with geometry defined in case 1. By this way, we aimed to check correctness of our triangular shaped coil simulations. Magnetic flux densities of triangular shaped coils at their center points analytically calculated by using our proposed method and the traditional method that exists in literature together with the flux densities calculated in the simulations are given in Table 4.3.1.1, Table 4.3.1.2, and Table 4.3.1.3 for various rounding amounts and coil side lengths equal to 7.5 cm, 16.0 cm, and 28.0 cm, respectively. In the tables, error between the results analytically found by using the proposed method and calculated in simulations is also given.

Arc start Point (cm, cm)	Magnetic Flux Density Calculated by Proposed Method (Wb/cm^2)	Magnetic Flux Density Calculated by Traditional Method (Wb/cm^2)	Magnetic Flux Density Calculated in Simulations (Wb/cm^2)	Error between Proposed Method Results and Simulation Results (%)
(0, 4.33)	2.4000E-05	2.4000E-05	2.4053E-05	0.22
(0.25, 3.89)	2.4048E-05	2.4048E-05	2.4063E-05	0.06
(0.50, 3.46)	2.4232E-05	2.4232E-05	2.4147E-05	0.35
(0.75, 3.03)	2.4630E-05	2.4630E-05	2.4644E-05	0.06
(1.00, 2.59)	2.5340E-05	2.5340E-05	2.5374E-05	0.14

Table 4.3.1.1 Calculated magnetic flux densities of triangular shaped coils in case 1 with a side length equal to 7.5 cm having different amounts of rounding.

Arc start Point (cm, cm)	Magnetic Flux Density Calculated by Proposed Method (Wb/cm^2)	Magnetic Flux Density Calculated by Traditional Method (Wb/cm^2)	Magnetic Flux Density Calculated in Simulations (Wb/cm^2)	Error between Proposed Method Results and Simulation Results (%)
(0, 9.23)	1.1253E-05	1.1253E-05	1.1253E-05	0.03
(0.25, 8.80)	1.1254E-05	1.1254E-05	1.1238E-05	0.14
(0.50, 8.37)	1.1270E-05	1.1270E-05	1.1312E-05	0.38
(0.75, 7.93)	1.1298E-05	1.1298E-05	1.1341E-05	0.38
(1.00, 7.50)	1.1343E-05	1.1343E-05	1.1393E-05	0.43
(1.25, 7.07)	1.1409E-05	1.1409E-05	1.1420E-05	0.10

Table 4.3.1.2 Calculated magnetic flux densities of triangular shaped coils in case 1 with a side length equal to 16.0 cm having different amounts of rounding.

Arc start Point (cm, cm)	Magnetic Flux Density Calculated by Proposed Method (Wb/cm^2)	Magnetic Flux Density Calculated by Traditional Method (Wb/cm^2)	Magnetic Flux Density Calculated in Simulations (Wb/cm^2)	Error between Proposed Method Results and Simulation Results (%)
(0, 16.16)	6.4285E-06	6.4285E-06	6.4301E-06	0.02
(0.25, 15.73)	6.4294E-06	6.4294E-06	6.4420E-06	0.20
(0.50, 15.29)	6.4320E-06	6.4320E-06	6.4306E-06	0.02
(0.75, 14.86)	6.4366E-06	6.4366E-06	6.4390E-06	0.04
(1.00, 14.43)	6.4435E-06	6.4435E-06	6.4852E-06	0.64
(1.25, 14.00)	6.4531E-06	6.4531E-06	6.4883E-06	0.54

Table 4.3.1.3 Calculated magnetic flux densities of triangular shaped coils in case 1 with a side length equal to 28.0 cm having different amounts of rounding.

When results are examined, it is seen that magnetic flux densities found in the simulations are very close to those analytically calculated. It indicates us that simulations are done correctly. In addition, error between the simulation results and the results

calculated by the proposed method is found to be less than 1%. This proves correctness of the proposed formulation.

4.3.2 Case 2 Results

We repeated our simulations for triangular shaped coils in case 2. Here, the triangular coil geometry is different from that in case 1 such that arcs at the corners are parts of different circles whose center points do not coincide with the mass center of triangle. As it is described in chapter 3, because of the unique geometry magnetic flux density created by the coil at its center point is not calculated by traditional formulas. Therefore, we calculated flux density by using our derived formulas for the coils in case 2.

To support our calculated results, we obtained simulations of the triangular shaped coils in case 2 having the same dimensions with the coils investigated in chapter 3. Magnetic flux densities of triangular shaped coils at their centers analytically calculated by using our proposed method and calculated in the simulations are given in Table 4.3.2.1, Table 4.3.2.2, and Table 4.3.2.3 for various rounding amounts and coil side lengths equal to 7.5 cm, 16.0 cm, and 28.0 cm, respectively. As in case 1, in the table error between the results is also given.

Arc start Point (cm, cm)	**Magnetic Flux Density Calculated by Proposed Method (Wb/cm^2)**	**Magnetic Flux Density Calculated in Simulations (Wb/cm^2)**	**Error between Proposed Method Results and Simulation Results (%)**
(0, 4.33)	2.4000E-05	2.4053E-05	0.22
(0.25, 3.89)	2.4018E-05	2.4127E-05	0.45
(0.50, 3.46)	2.4082E-05	2.4033E-05	0.20
(0.75, 3.03)	2.4213E-05	2.4057E-05	0.65
(1.00, 2.59)	2.4443E-05	2.4488E-05	0.19

Table 4.3.2.1 Calculated magnetic flux densities of triangular shaped coils in case 2 with a side length equal to 7.5 cm having different amounts of rounding.

Arc start Point (cm, cm)	**Magnetic Flux Density Calculated by Proposed Method (Wb/cm^2)**	**Magnetic Flux Density Calculated in Simulations (Wb/cm^2)**	**Error between Proposed Method Results and Simulation Results (%)**
(0, 9.23)	1.1251E-05	1.1253E-05	0.03
(0.25, 8.80)	1.1252E-05	1.1286E-05	0.31
(0.50, 8.37)	1.1257E-05	1.1294E-05	0.32

(0.75, 7.93)	1.1268E-05	1.1243E-05	0.22
(1.00, 7.50)	1.1283E-05	1.1284E-05	0.01
(1.25, 7.07)	1.1305E-05	1.1314E-05	0.08

Table 4.3.2.2 Calculated magnetic flux densities of triangular shaped coils in case 2 with a side length equal to 16.0 cm having different amounts of rounding.

Arc start Point (cm, cm)	**Magnetic Flux Density Calculated by Proposed Method (Wb/cm^2)**	**Magnetic Flux Density Calculated in Simulations (Wb/cm^2)**	**Error between Proposed Method Results and Simulation Results (%)**
(0, 16.16)	6.4285E-06	6.4301E-06	0.02
(0.25, 15.73)	6.4289E-06	6.4616E-06	0.51
(0.50, 15.29)	6.4299E-06	6.4242E-06	0.09
(0.75, 14.86)	6.4316E-06	6.3806E-06	0.80
(1.00, 14.43)	6.4341E-06	6.4500E-06	0.25
(1.25, 14.00)	6.4376E-06	6.4686E-06	0.48

Table 4.3.2.3 Calculated magnetic flux densities of triangular shaped coils in case 2 with a side length equal to 28.0 cm having different amounts of rounding.

When results are examined, it is again seen that simulation results are very close to the results calculated by the proposed method. And similar to case 1, the amount of error in terms of percentage is lower than 1%. This proves the correctness of the proposed formulations for the triangular coils.

4.4 Summary

In this chapter, the coils whose parameters formerly determined by the proposed formulizations were simulated. To simulate these coils computer-based software tool CST Studio was used. The coil shapes are selected as squircle and triangular to be able to compare the results calculated in previous chapters. For each coil shape two different cases were examined, and for each case simulations were repeated with the coils having different amounts of rounding. Magnetic flux densities found in simulations were compared with magnetic flux densities calculated by using both proposed and traditional methods. When all results are examined, it is seen that, maximum error is below 1%, which demonstrates correctness of the derived formulas.

Chapter 5

Conclusions and Future Prospects

5.1 Conclusion

Coils form an important part of induction heating systems. Commonly used coil shapes in industry are square and circular shapes. However, due to the production difficulties of coils that have sharp corners, it is possible to face with square shaped coils having rounded corners, which are called squircle coils. In some applications, on the other hand, squircle coils are preferred because of their geometry-based properties. Since magnetic flux densities created by the coils and their inductance values are crucial for induction heating system performance, it is important to calculate magnetic flux densities and inductance of a coil at design phase before production. In this way, it is possible to avoid design errors before production. However, these calculations can be done analytically by using conventional formulizations only for coils that have regular shapes such as square and circular shaped coils, etc.

In this thesis, to fill the gap in the literature we obtained analytical derivations for coils that have rounded corners. We obtained formulas to calculate geometrical parameters and magnetic flux density created by coils having rounded corners. By using the formulas that we derived for the first time in literature, the magnetic field created by not only regular shaped coils but also coils that have rounded corners can be calculated. Analytical calculation of magnetic flux density, which is related with the inductance, enables to understand change of flux density created by the coil with rounding of the coil corners. Therefore, before production, with the proposed method and derived formulas in this study it will be possible to detect design errors for coils having rounded corners.

We obtained our derivations for square and triangular shaped coils with rounded corners. To prove our derivations, by using the derived formulas magnetic flux densities

at the center point of squircle and triangular shaped coils were calculated. For each coil shape two different geometries were investigated. In the first case, arcs at the coil corners are parts of the same circle and center of the circle coincides with the center of the coil. In the second case, on the other hand, arcs are parts of circles positioned at different locations such that centers of these circles do not coincide with the center of the coil. Calculations were repeated in each case for the coils having three different sizes, and for each size various amounts of rounding were selected. To verify the results, magnetic flux densities were calculated for the coils having geometries as in case 1 by using traditional formulas exist in literature. Comparison of the results that were found by using our derived formulas and the traditional formulas shows that the calculated magnetic flux densities are almost the same. Calculated errors between the results found with the proposed and conventional methods are very low, and due to finite precision of in our calculations.

After proving correctness of the derived formulas by comparing magnetic flux density results calculated in case 1 with the proposed and traditional methods, simulations were conducted for the coils same with those analytically investigated. Since the coil geometries in case 2 are different and magnetic flux densities generated by these coils at their centers are calculated only with the formulas that we derived, it is necessary to verify the results that we analytically calculated for the coils in the second cases. To this end, magnetic flux densities generated by square and triangular shaped coils having rounded corners were calculated with simulations for not just case 1 but also case 2. After comparing the results that were analytically calculated and found with simulations, it is seen that in all the cases simulation results support the results that we calculated analytically with our proposed and conventional methods. Error between the proposed method results and the simulation results are found to be very low, i.e., far below 1%.

In short, in this thesis, alternative formulizations to conventional ones are proposed and proved to calculate magnetic field created at the center of planar coils. The proposed method and derived formulas are applicable to not only regular shaped coils such as circular and square shaped coils but also irregular shaped coils such as squircle and triangular shaped coils with rounded corners. With the derived formulas magnetic flux density change due to rounding at the corners are analytically calculated. It means, before production, it is possible to calculate change of magnetic field and flux created by a coil as a result of rounding at its corners.

5.2 Future Prospects

In this study, squircle and triangular shaped coils were examined analytically and with simulations. As a future work, it is planned to manufacture the coils that we analytically investigated in this study. After manufacturing the coils, magnetic flux density created by them will be measured.

In addition, since the formulas derived in this study form a basis for inductance calculation of different shaped coils having rounded corners, we are also planning to extend our derivations to obtain formulas to analytically calculate inductance values of the coils. After derivations and analytical calculations, in the future, we will determine inductance of the coils both with simulations and experiments.

BIBLIOGRAPHY

[1] M. Sweeney, J. Dols, B. Fortenbery, F. Sharp, “Induction Cooking Technology Design and Assessment,” ACEEE Summer Study on Energy Efficiency in Buildings, 9-370 (2014).

[2] N. Chuang, J. Lin, T. Chang, T. Tsai, K. Chang, C. Wu, "The Film Thickness Effect on Electrical Conduction Mechanisms and Characteristics of the Ni–Cr Thin Film Resistor," IEEE Journal of the Electron Devices Society, vol. 4, no. 6, pp. 441-444, (2016).

[3] F. K. Chowdhury, H. Pourzand and M. Tabib-Azar, "Investigation of contact resistance evolution of Ir, Pt, W, Ni, Cr, Ti, Cu and Al over repeated hot-contact switching for NEMS switches," IEEE 26th International Conference on Micro Electro Mechanical Systems (MEMS), pp. 445-448 (2013).

[4] H. Kajimoto and L. A. Jones, "Wearable Tactile Display Based on Thermal Expansion of Nichrome Wire," in IEEE Transactions on Haptics, vol. 12, no. 3, pp. 257-268 (2019).

[5] C. D. Starr and T. P. Wang, "The electrical characteristics of a nickel-chromium-aluminium-copper resistance wire," in Proceedings of the IEE - Part B: Radio and Electronic Engineering, vol. 104, no. 17, pp. 515-518 (1957).

[6] A. Pyzyna et al., "Resistivity of copper interconnects at 28 nm pitch and copper cross-sectional area below 100 nm2," 2017 IEEE International Interconnect Technology Conference (IITC), pp. 1-3 (2017).

[7] S. Passon, I. Gitin and J. Meisner, "Investigating the properties of precision resistors for the application in high voltage DC dividers," 2016 IEEE International Workshop on Applied Measurements for Power Systems (AMPS), pp. 1-6 (2016).

[8] E. Grundkötter, P. Weßkamp and J. Melbert, "Transient Thermo-Voltages on High-Power Shunt Resistors," in IEEE Transactions on Instrumentation and Measurement, vol. 67, no. 2, pp. 415-424 (2018).

[9] N. Fletcher, M. Götz, R. Goebel and B. Rolland, "On the definition of DC in resistance measurements," 29th Conference on Precision Electromagnetic Measurements (CPEM 2014), pp. 688-689 (2014).

[10] https://cooking.stackexchange.com/questions/58307/is-it-safe-to-leave-a-broth-simmering-overnight-on-an-electric-stove/93916/ (15.10.2019)

[11] O. Lucía, P. Maussion, E. J. Dede and J. M. Burdío, "Induction Heating Technology and Its Applications: Past Developments, Current Technology, and Future Challenges," in IEEE Transactions on Industrial Electronics, vol. 61, no. 5, pp. 2509-2520 (2014).

[12] R. P. Wojda and M. K. Kazimierczuk, "Analytical winding size optimisation for different conductor shapes using Ampere's law," in IET Power Electronics, vol. 6, no. 6, pp. 1058-1068 (2013).

[13] N. R. Stansel, "Induction heating — Selection of frequency," in Electrical Engineering, vol. 63, no. 10, pp. 755-759 (1944).

[14] H. F. Storm, "Surface Heating by Induction," in Transactions of the American Institute of Electrical Engineers, vol. 63, no. 10, pp. 749-755 (1944).

[15] https://www.hflitzwire.com/litz-wire-theory-and-principle/ (17.10.2019)

[16] J. Acero et al., "The domestic induction heating appliance: An overview of recent research," 2008 Twenty-Third Annual IEEE Applied Power Electronics Conference and Exposition, pp. 651-657 (2008).

[17] M. E. Tulu and D. Yildirim, "Induction cooker design with quasi resonant topology using jitter drive method," 2013 12th International Conference on Environment and Electrical Engineering, pp. 1-6 (2013).

[18] A. Shenkman, B. Axelrod and Y. Berkovich, "Improved modification of the single-switch AC-AC converter for induction heating applications," in IEE Proceedings - Electric Power Applications, vol. 151, no. 1, pp. 1-4 (2004).

[19] https://electronicsforu.com/resources/induction-cooker-working/2 (10.10.2019)

[20] Clayton R. Paul, Introduction to Electromagnetic Compatibility (Wiley Series in Microwave and Optical Engineering), Wiley-Interscience, 2006

[21] R. J. Plowman, "Conducted EMC testing a review and introduction," IEE Colloquium on EMC Testing for Conducted Mechanisms, pp. 1/1-1/9 (1996).

[22] S. Wang, K. Izaki, I. Hirota, H. Yamashita, H. Omori and M. Nakaoka, "Induction-heated cooking appliance using new quasi-resonant ZVS-PWM inverter with power factor correction," in IEEE Transactions on Industry Applications, vol. 34, no. 4, pp. 705-712 (1998).

[23] O. Lucía, J. M. Burdío, I. Millán, J. Acero and L. A. Barragán, "Efficiency-Oriented Design of ZVS Half-Bridge Series Resonant Inverter With Variable Frequency Duty Cycle Control," in IEEE Transactions on Power Electronics, vol. 25, no. 7, pp. 1671-1674 (2010).

[24] G. A. Covic and J. T. Boys, "Inductive Power Transfer," in Proceedings of the IEEE, vol. 101, no. 6, pp. 1276-1289 (2013).

[25] N. Alireza, M. Javad, M. Jafar, “A Current-Fed Parallel Resonant Push-Pull Inverter with a New Cascaded Coil Flux Control for Induction Heating Applications,” Journal of Power Electronics. 11. 10.6113/JPE.2011.11.5.632, (2011).

[26] K. A. Nugroho, B. R. Septiawan, G. Hersanto and F. I. Hariadi, "Development of ARM Microcontroller-based Quasi-Resonant inverter Induction Heater," 2016 3rd Conference on Power Engineering and Renewable Energy (ICPERE), pp. 201-208 (2016).

[27] O. Jimenez, O. Lucia, I. Urriza, L. A. Barragan and D. Navarro, "Design and Evaluation of a Low-Cost High-Performance$ \Sigma$–$\Delta$ADC for Embedded Control Systems in Induction Heating Appliances," in IEEE Transactions on Industrial Electronics, vol. 61, no. 5, pp. 2601-2611 (2014).

[28] N. Booma, S. Rama, V. Pradeep, “Power Tracking Control of Domestic Induction Heating System using Pulse Density Modulation Scheme with the Fuzzy Logic Controller,” Journal of Electrical Engineering and Technology. vol. 9. 10.5370/JEET.2014.9.6.1978. (2014)

[29] J. A. Becker, C. B. Green and G. L. Pearson, "Properties and Uses of Thermistors--- Thermally Sensitive Resistors," in Transactions of the American Institute of Electrical Engineers, vol. 65, no. 11, pp. 711-725 (1946).

[30] http://www.egoproducts.com/en/products/appliance-heating/induction/ (12.10.2019)

[31] R. M. Baker, "Design and calculation of induction heating coils," in Electrical Engineering, vol. 76, no. 2, pp. 149-149 (1957).

[32] T. Isobe, K. Usuki, N. Arai, T. Kitahara, K. Fukutani and R. Shimada, "Variable frequency induction heating using magnetic energy recovery switch (MERS)," 2008 IEEE Power Electronics Specialists Conference, pp. 2139-2145 (2008).

[33] J. Acero, C. Carretero, I. Millán, Ó. Lucía, R. Alonso and J. M. Burdío, "Analysis and Modeling of Planar Concentric Windings Forming Adaptable-Diameter Burners for Induction Heating Appliances," in IEEE Transactions on Power Electronics, vol. 26, no. 5, pp. 1546-1558 (2011).

[34] F. Forest, S. Faucher, J. Gaspard, D. Montloup, J. Huselstein and C. Joubert, "Frequency-Synchronized Resonant Converters for the Supply of Multiwinding Coils in Induction Cooking Appliances," in IEEE Transactions on Industrial Electronics, vol. 54, no. 1, pp. 441-452 (2007).

[35] C. Cheng, H. Wei, L. Jun, L. Yu, T. Qing, Z. Xinyu, S. Hongshi, X. Changsheng, “Planar micro-nano-coils for electrically driving liquid crystal microlenses based on wireless power transmission,” 981105. 10.1117/12.2204807 (2015).

[36] M. F. Erman and V. T. Kilic, "Magnetic Field Calculation of Square Coils Having Rounded Corners," 2019 1st Global Power, Energy and Communication Conference (GPECOM), pp. 212-215 (2019).

[37] B. Patidar, M. M. Hussain, S. K. Jha, A. Sharma and A. P. Tiwari, "Analytical, numerical and experimental analysis of induction heating of graphite crucible for melting of non-magnetic materials," IET Electric Power Applications, vol. 11, no. 3, pp. 342-351 (2017).

[38] V. T. Kilic, E. Unal, N. Yilmaz and H. V. Demir, "All-Surface Induction Heating with High Efficiency and Space Invariance Enabled by Arraying Squircle Coils in Square Lattice," IEEE Transactions on Consumer Electronics, vol. 64, no. 3, pp. 339-347 (2018).

[39] E. Ünal, V. T. Kilic, H. V. Demir, "Inductive coil unit comprising conductive layers," Turkish Patent TR201615831, International Patent WO2018083058 (2018)

[40] V. T. Kilic, E. Unal, E. Gonendik, N. Yilmaz and H. V. Demir, "Strongly Coupled Outer Squircle–Inner Circular Coil Architecture for Enhanced Induction Over Large Areas," in IEEE Transactions on Industrial Electronics, vol. 63, no. 12, pp. 7478-7487 (2016).

[41] D. K. Cheng, "Field and Wave Electromagnetics," 2nd Edition, Addison Wesley, Inc., pp. 547- 557 (1989).

[42] A. Rerkratn, W. Petchmaneelumka, J. Kongkauroptham, K. Kraisoda and A. Kaewpoonsuk, "Pulse Induction Metal Detector Using Sample and Hold Method," 11th International Conference on Control, Automation and Systems, Gyeonggi-do, pp. 45-48 (2011).

[43] A. C. Lahrech, A. Zaoui, F. Benyoubi and A. Sakoub, "Modeling of inductive metal detector with swept frequency excitation," 2013 International Conference on Electromagnetics in Advanced Applications (ICEAA), Torino, pp. 1305-1308 (2013).

[44] Nelson, C.V, "Metal detection and classification technologies," Johns Hopkins APL technical digest. 25 (1). p.pp. 62–67 (2004).

[45] T. Watanabe, S. Nagaya, N. Hirano and S. Fukui, "Elemental Development of Metal Melting by Electromagnetic Induction Heating Using Superconductor Coils," in IEEE Transactions on Applied Superconductivity, vol. 26, no. 3, pp. 1-4, April 2016, Art no. 3700504.

[46] A. Gasiorski, P. Kielbasa and Z. Posylek, "Inverter with 280 kHz frequency to induction levitation of metal melting in a vacuum," 2018 Applications of Electromagnetics in Modern Techniques and Medicine (PTZE), Racławice, pp. 53-56 (2018).

[47] https://ultraflexpower.com/induction-heating/ (25.12.2019).

[48] Z. Zhang, H. Pang, A. Georgiadis and C. Cecati, "Wireless Power Transfer—An Overview," in IEEE Transactions on Industrial Electronics, vol. 66, no. 2, pp. 1044-1058, (2019).

[49] https://www.rs-online.com/designspark/wireless-power-transfer-system-for-rehabilitation (26.12.2019).